$^{87}Sr/^{86}Sr$ in plagioclase, evidence for a crustal origin of the Hakefjorden Complex, SW Sweden

Alexandra Glommé

Dissertations in Geology at Lund University,
Master's thesis, no 453
(45 hp/ECTS credits)

Department of Geology
Lund University
2015

$^{87}Sr/^{86}Sr$ in plagioclase, evidence for a crustal origin of the Hakefjorden Complex,

SW Sweden

Master's thesis

Alexandra Glommé

Department of Geology
Lund University
2015

Contents

Cover Picture: Anorthosite blocks in a norite matrix from Älgön. Photo: Alexandra Glommé

$^{87}Sr/^{86}Sr$ in plagioclase, evidence for a crustal origin of the Hakefjorden Complex, SW Sweden

ALEXANDRA GLOMMÉ

Glommé, A., 2015: Isotopic, petrological and geochemical description of plagioclase, deciding origin of the Hakefjorden Complex, SW Sweden. *Dissertations in Geology at Lund University*, No. 453, 31 pp. 45 hp (45 ECTS credits).

Abstract: The studied intrusion, the Hakefjorden Complex on Älgön is a norite-anorthosite complex situated in the archipelago on the west coast of Sweden. The origin of the intrusion will be deduce through *in situ* Sr-isotope analysis by MC-ICP-MS (multiple collector- inductively coupled plasma- mass spectrometry) on plagioclase, together with petrographic description and chemical analysis. The examined plagioclase includes megacrysts and matrix crystals in the different rock units. Sr-isotopic results show that the magma is homogenous, with only small variations in the initial $^{87}Sr/^{86}Sr$ with an average of 0.7050 for the majority of rock units. The mafic enclave is the only one that distinguishes itself from the rest with higher values in the initial $^{87}Sr/^{86}Sr$, and a significantly more crustal signature. The anorthite (An) values shows more variation between the rock units and plagioclase types than the Sr. The An-variation indicates a crystallization sequence where the IRL-matrix plagioclase crystallizes first. Oscillatory variation of both initial Sr-ratio and An is seen in several of the plagioclase megacrysts. The Sr-ratio show that little contamination has occurred during crystallization and emplacement of the intrusion, and that the mafic enclave is not similar to the rest of the Hakefjorden Complex rock units. The combined results show that a polybaric evolution is most likely, with little contamination from crustal components or other magmas.

Keywords: Plagioclase, Älgön, Hakefjorden complex, Sweden, MC-ICP-MS, Sr-isotopes, SEM, Geochemistry

Supervisor: Anders Scherstén

Subject: Bedrock Geology

Alexandra Glommé, Department of Geology, Lund University, Sölvegatan 12, SE-223 62 Lund, Sweden. E-mail: glomme_@hotmail.com

$^{87}Sr/^{86}Sr$ i plagioklas, bevis för krustalt ursprung för Hakefjorden-komplexet, SV Sverige

ALEXANDRA GLOMMÉ

Glommé, A., 2015: Isotop, petrologisk och geokemisk beskrivning av plagioklas, för bestämning av Hakefjordens ursprung, SV Sverige. *Examensarbeten i geologi vid Lunds universitet*, Nr. 453, 31 sid. 45 hp.

Sammanfattning: Den studerade intrusionen, Hakefjordenkomplexet på Älgön är ett norit anortosit komplex som ligger i skärgården på Sveriges västkust. Genom *in situ* Sr-isotop analyser av MC-ICP-MS (multiple collector- inductively coupled plasma- mass spectrometry) på plagioklas, tillsammans med petrografisk beskrivning och kemiska analyser ska det förhoppningsvis bli klarhet i intrusionens ursprung. Plagioklasen som undersöks är megakryster, och matrix kristaller i de olika bergarterna. Sr-isotop resultaten visar att magman är homogen, med bara små variationer i initiala $^{87}Sr/^{86}Sr$ och ett medelvärde på 0,7050 för majoriteten av bergarterna. Det är bara den mafiska enclaven som urskiljer sig från resten med högre initiala $^{87}Sr/^{86}Sr$ och betydligt större krustal signatur. Anortit (An)-halten varierar stort mellan olika bergarterna och plagioklas typer jämfört med Sr-kvoterna. An-variationen visar kristallisations sekvensen där matrix plagioklasen i den ilmenit rika noriten är tidig. Variation i både Sr-kvoterna och An-halt finns i flera av plagioklas megakrysterna. Sr-kvoterna visar att lite kontamination har skett under intrusionen, och att den mafiska enklaven inte liknar någon av de andra bergarterna i Hakefjorden Komplexet. De kombinerade resultaten visar troligen på en polybarisk evolution utan magma mixing eller annan kontamination från omkringliggande krustala bergarter.

Nyckelord: Plagioklas, Älgön, Hakefjorden , Sverige, MC-ICP-MS, Sr-isotoper, SEM, Geokemi

Handledare: Anders Scherstén

Ämnesområde: Berggrundsgeologi

Alexandra Glommé, Geologiska institutionen, Lunds Universitet, Sölvegatan 12, 223 62 Lund, Sverige. E-post: glomme_@hotmail.com

1 Introduction

Älgön together with Brattön are part of a norite-anorthosite intrusion post-dating the Sveonorwegian orogeny (Fig. 1; Årebäck 1995). The intrusion is called the Hakefjorden Complex, after Ljungner (1927) (Årebäck 1995; Årebäck & Stigh 1997, 2000). The Hakefjorden Complex intruded into the Stora Le-Marstrand formation (SLM), which is made up of gneisses, metasediments and metavolcanics in the Idefjorden terrane (Lundquist 1979; Årebäck 1995; Petersson *et al*. 2015).

The island is a beautiful natural reserve and a fascinating geological site, attracting much attention from both scientists and hikers throughout the years (Årebäck 1995; Årebäck & Stigh 1997, 2000; Fahlén *et al*. 2008). The Hakefjorden Complex is an adcumulate rock complex (Winter 2010; Årebäck 1995) with anorthosite blocks found in a fine grained norite matrix. The norite contains an ilmenite-rich leuconorite (IRL) which has high concentrations of Fe/Ti-oxides compared to the norite. Along the contact monzonorite, contact migmatites and a hybrid rock with mafic enclaves are found (Fig. 2).

Many different theories regarding parental magma, tectonic setting and emplacement of anorthosite complexes have been debated for a long time (Duchesne *et al*. 1999; Markl & Höhndorf 2003; Vander Auwera *et al*. 2011; Bybee *et al*. 2014; Chen *et al*. 2015).

In many anorthosite complexes over the world High Aluminium Orthopyroxene Megacrysts (HAOM) are common. They are good indicators for high pressure and give clues about the parental magma origin, and composition (Panjasawatwong *et al*. 1995; Duchesne *et al*. 1999; Wiszniewska *et al*. 2002; Charlier *et al*. 2010; Vander Auwera *et al*. 2011; Bybee *et al*. 2014; Chen *et al*. 2015).

Sr-isotopes and An-content in plagioclase are indicators of changes in pressure, temperature and chemistry of melts, which are all important factors for understanding emplacement and origin for anorthosite complexes (Panjasawatwong *et al*. 1995; Blundy & Wood 1991; Vander Auwera *et al*. 2000, 2011; Charlier *et al*. 2010; Ustunisik *et al*. 2014; Chen *et al*. 2015).

In this study, *in situ* MC-ICP-MS (multiple collector- inductively coupled plasma- mass spectrometry) is used for investigations of $^{87}Sr/^{86}Sr$ variation together with chemistry and petrographic description on different types of plagioclase.

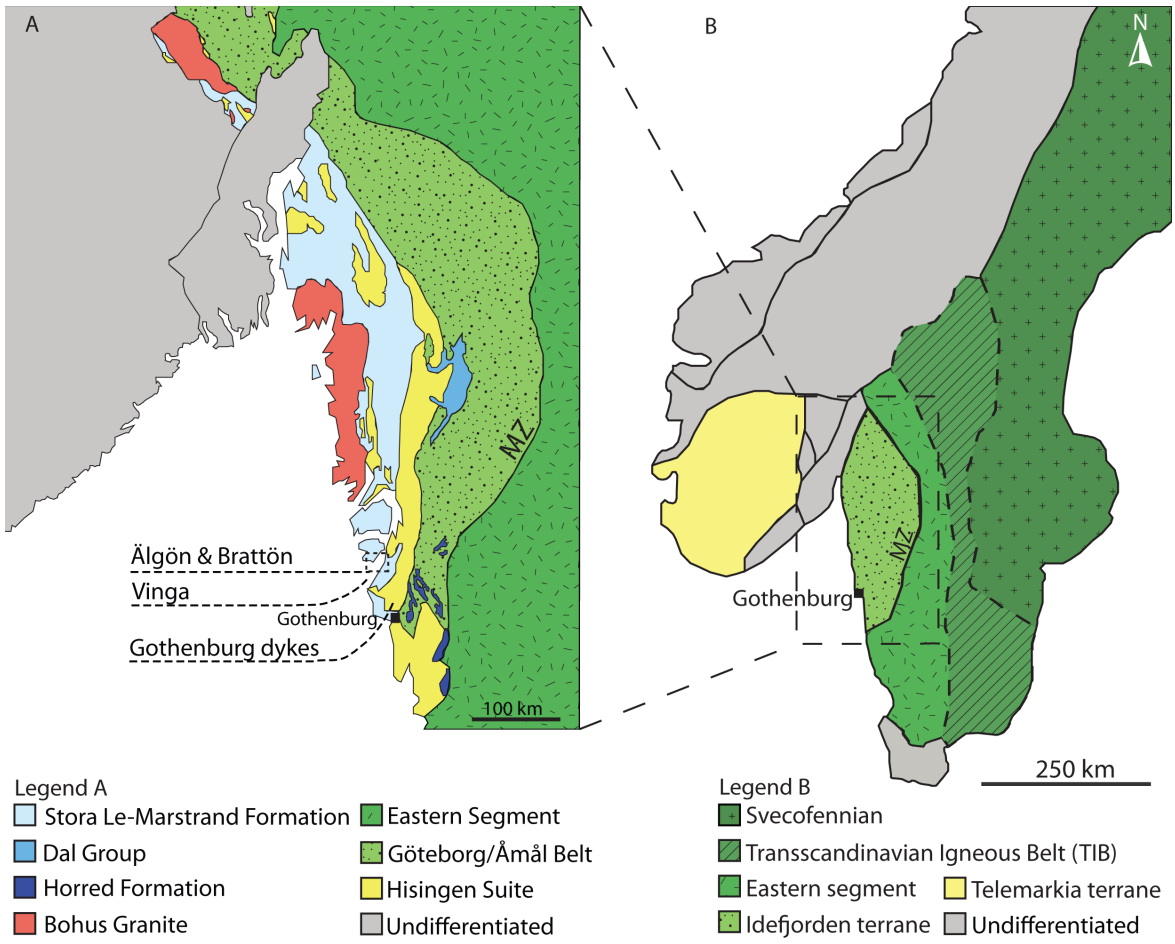

Fig. 1. Illustrates the regional geology in Sweden and Norway. MZ illustrates the Mylonite Zone. A) Zoomed in picture showing the west coast of Sweden and the locations for the late stage intrusions. Based on a figure by Petersson *et al.* (2014). B) Illustrates the different orogenic belts through Sweden and part of Norway. TIB is marked with dashed lines as it's not entirely accepted as an own belt. Based on a figure by Åhäll & Connelly (2008).

Fig. 2. The figure illustrate Älgöns different rock units and their relation to each other are shown together with the outcrop area for the intrusion. Based on mapping and model by Årebäck (1995).

The aims of this study include:

- Understanding the origin and magmatic evolution of the Hakefjorden Complex.
- Deduce source of the parental magma.
- To unravel the differentiation sequence of the rock units, through An and Sr-isotopic ratio variation in plagioclase.
- Evaluate contamination such as of magma mixing, mingling or crustal assimilation occurred.

Hopefully it will also lead to a better understanding of the origin of these anorthosite complexes world wide.

2 The origin of massif-type anorthosite

The ongoing debate considering petrogenesis of massi-type anorthosites has continued for a long time and is still controversial (Bybee *et al*. 2014 and sources therein). Chen *et al*. (2015) summarize the different possibilities of tectonic setting and parental magma for these kinds of units. The most common theories regarding these include a lower crust and mantle mixing, (Markl & Höhndorf 2003) partial melting of continental arc roots (Duchesnes *et al*. 1999; Vander Auwera *et al*. 2011) and long lived convergent arc setting (Bybee *et al*. 2014). The emplacement and formation for massif-type anorthosite complexes are debated as well, but the most widely accepted theory is a polybaric evolution. Massif-type anorthosite complexes are adcumulate rocks. The plagioclase crystallizes at depth and starts accumulating at the top of the magma chamber due to lower density. The crystal-mush will then start rising due to gravitational instability (Årebäck 1995; Duchesnes *et al*. 1999; Winter 2010; Chen *et al*. 2015). These types of massif anorthosites are often related to mafic host rocks such as high Al basaltic liquids, primitive orthopyroxene monzonorites with plausible lower crustal source or mafic plutons (Longhai *et al.* 1999; Vander Auwera *et al.* 2011).

2.1 Plagioclase zoning

If the crystals form during stable conditions with little or no change in temperature or pressure the zoning will be normal. Normal zoning is when the core is more Ca rich and the rim is more Na rich (Winter 2010). In this case, the zoning is caused by the variation in An content, affected by other phases crystallizing. Reversed zoning going from Na-rich to Ca-rich is common in metamorphic plagioclase, when the crystallization is associated with rising temperature (Winter 2010). If convection currents are present in the magma this can make the crystals develop an oscillatory zoning (Ustunisik *et al*. 2014). The most common reason for oscillatory zonation is when the An content decrease in a uneven pace (Winter 2010). The zoning can also develops as the plagioclase crystal travels up and down in the magma chamber. The zoning develops as the An content in plagioclase is pressure dependent (Fig. 3). The crystal will incorporate Ca or Na depending on if it's going up or down in the chamber

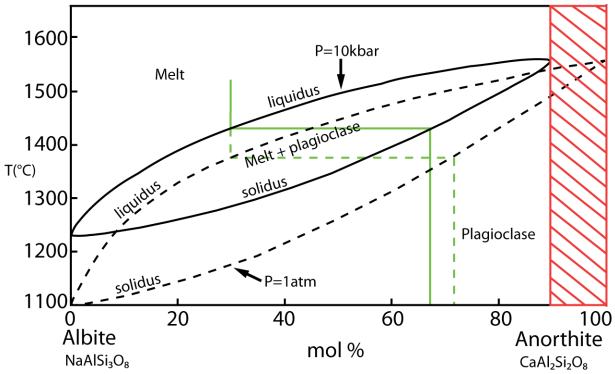

Fig. 3. The figure illustrates the cooling of a magma with the same initial An-content but crystallizing at different pressures. At 10 kbar the An-content will be lower than at 1 atm, because of the reasons mentioned in the text. The red area is to complex and is not included in this study. Modified after Lindsley (1971).

(Panjasawatwong *et al*. 1995; Ustunisik *et al*. 2014). Chemistry and zonation of plagioclase can deduce how the plagioclase crystallized, origin, parental magma, magma mixing and contamination (Vander Auwera *et al*. 2011; Chen *et al*. 2015). This will be explained in further detail later on.

2.2 Sr-isotopes and An-content

Sr-isotope variation and An-content in plagioclase is dependent on chemistry of the magma, pressure, temperature, as well as and H_2O content of the magma (Longhi *et al.* 1993; Panjasawatwong *et al*. 1995; Charlier *et al*. 2010; Ustunisik *et al*. 2014; Chen *et al*. 2015). These latter factors are responsible for smaller changes in the An-content, ±5% which Panjasawatwong *et al*. (1995) and Ustunisik *et al*. (2014) showed in their experiments. The chemistry of the melt, regarding Ca# and Al# are probably the factors affecting the An-content the most (Panjasawatwong *et al*. 1999; Ustunisik *et al*. 2014).

Fractional crystallization based on Bowen's reaction series (1922) and his theories behind it show that the minerals forming have a predestined chemistry. The first plagioclase grain to crystallize will have a higher An-content than later crystals forming, hence normal zoning.

If there is more than plagioclase crystallizing as a calcic phase, the crystal chemistry becomes more temperature dependent (Ustunisik *et al*. 2014). With more than one phase saturated in the system its more sensitive to changes in temperature, affecting the minerals. This could mean that the partitioning between Ca and Na will be magnified in the plagioclase crystallization (Ustunisik *et al.* 2014).

Sr-isotopes are used because they are more compatible in plagioclase compared to other minerals. The reason why Sr is compatible in plagioclase is that ^{87}Rb will decay to ^{87}Sr and as the Rb/Sr partition coefficient is extremely low in plagioclase, Sr is suitable for plagioclase. When plagioclase crystallize it does not differentiate between isotopes but include them all in the same amount. This means that the ratio in the crystal will be the same as in the parental magma, also recording any changes in Sr concentration due to contamination or magma mixing. Blundy & Wood (1991) showed that the Sr partitioning between crystal and coexisting liquid is influenced by the albite (Ab) and An content in the plagioclase, making Sr-isotopes more compatible in Ab-rich palgiocalse. They concluded that the crystal chemistry is the most important factor deciding the Sr-content, making temperature, pressure or fluid composition minor factors. The reason that Sr-isotopes favor Ab-rich plagioclase over An-rich is because of the higher elasticity in Ab-rich plagioclase. The difference in size between the sodium and calcium ions also makes Sr-isotopes favor Ab-rich plagioclase. Thus the Sr content is correlated with higher Ab rather than high An content (Blundy & Wood 1991). The Sr in the liquid can be calculated due to this correlation and is important when trying to unravel igneous progressions (Blundy & Wood 1991).

This is valuable information when trying to decide the origin and emplacement for anorthosite complexes. The Sr-isotope variation and An content can be linked to several important environments. Decompression and low pressure will give higher An-values, higher Sr concentration with lower pressure, more Sr in more sodic crystals, higher Sr concentration with decrease in temperature, together with more heterogeneous Sr-isotope distribution in the crystal (Blundy & Wood 1991; Vander Auwera *et al*. 2000; Charlier *et al*. 2010; Vander Auwera *et al*. 2011; Ustunisik *et al*. 2014; Chen *et al*. 2015). Contamination can be seen in higher Sr-isotope ratios as the mantle has low ratios and higher Sr ratios will indicate a more crustal signature (Fig. 4). Looking at the Sr variation after a melt has initiated from CHUR (chondritic uniform reservoir) the crust will become gradually enriched as the mantle will become depleted (Fig. 4).

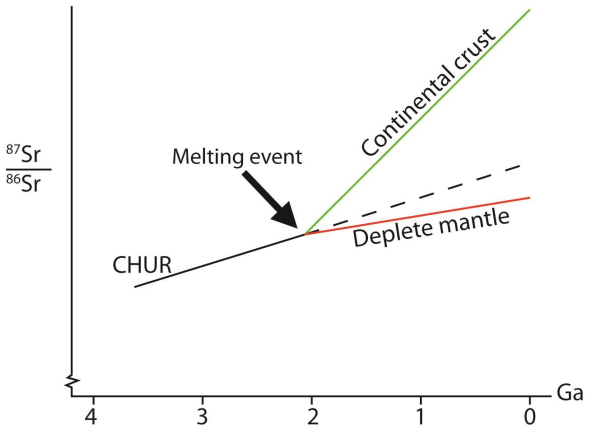

Fig. 4. The general trend looking at Sr variation over time, with CHUR as origin. The depleted mantle will fall below the predicted trend for the CHUR and the Continental crust will be more enriched. The continental crust will become gradually more enriched in $^{87}Sr/^{86}Sr$ while the depleted mantle will have low $^{87}Sr/^{86}Sr$ values.

2.3 HAOM

Later studies have shown that High Aluminium Orthopyroxene Megacrysts (HAOM) often is associated with plagioclase megacrysts in anorthosite complexes, indicating high pressure and polybaric evolution of the complex. High pressure is needed for the HAOM to be stable and crystallize together with plagioclase megacrysts, since it's a plagioclase saturated melt (Duchesne *et al*. 1999; Longhi *et al.* 1999; Vander Auwera *et al*. 2000; Wiszniewska *et al*. 2002; Charlier *et al.* 2010; Vander Auwera *et al*. 2011; Bybee *et al*. 2014; Chen *et al*. 2015).

For the HAOM to form in a plagioclase saturated magma, pyroxene stability is needed. This can only happen at high pressures (Duchesne *et al*. 1999; Char-

lier *et al*. 2010; Vander Auwera *et al*. 2011; Bybee *et al*. 2014; Chen *et al*. 2015). Another requirement for both plagioclase and orthopyroxene megacrysts to crystallize together is a high Al magma (Schiellerup *et al*. 2000).

3 Geologic setting

The geology in Sweden is complex with many different orogenic and magmatic events, during which the rocks have been metamorphosed, folded and altered. Below is a description of the rock units and evolution of SW Sweden.

3.1 Pre-Sveconorwegian rocks

The Svecokarelian orogeny is found east of the younger Sveconorwegian orogeny (Fig. 1) (Gorbatschev & Bogdana 1993; Söderlund *et al.* 2005; Petersson *et al*. 2015). The Svecokarelian orogeny is made up of 2.1–1.89 Ga Svecofennian basement rocks, including metasupracrustals and plutonic intrusions such as the Transcandinavian Igneous Belt (TIB). TIB is the youngest part of the Svecokarelian orogeny and is made up of 1.89–1.66 Ga granite and syenite batholits with minor mafic rocks, and are the youngest and most easterly Svecofennian rocks. Later intrusions ranging in age from 1.65–0.95 Ga such as dolerites and granite plutons have intruded TIB (Gorbatschev & Bogdana 1993; Söderlund *et al.* 1999; Söderlund *et al.* 2005; Möller *et al.* 2007; Petersson *et al*. 2015).

The rock within the Sveconorwegian Idefjorden terrane are of Pre-Sveconorwegian age and include, the Horred formation which is the oldest at 1.66 Ga and consist metamorphosed supracrustal, dominantly metavolcanics. The Åmål formation is 1.63–1.59 Ga and is composed of volcanics and sediments metamorphosed in greenschist to amphibolite-facies (Brewer *et al.* 1998; Åhäll *et al*. 1998; Åhäll & Connelly 2008; Petersson *et al*. 2015). SLM consist of metamorphosed greywacke metasediments together with subordinate mafic intrusions and metavolcanics. It was migmatized during Gothian orogeny, in amphibolite facies and again during the Sveconorwegian orogeny but during this time the metamorphism was mainly in shear zones (Bergström 1963; Åhäll 1995; Åhäll & Daly 1989; Åhäll *et al.* 1998; Åhäll & Connely 2008). Åhäll *et al.* (1998) dated the deposition and accreation of the SLM to the Baltic shield to 1598–1587 ±3 Ma. Older igneous activity in the SLM arc system is dated to have started around 1630 Ma (Åhäll *et al.* 1998). Brewer *et al.* (1998) argue that the SLM and its metavolcanics formed in an island arc.

The Telemarkian terrane together with the other Norwegian terranes are located west of the Idefjorden terrane. They are made up of orthogneisses and have an age around 1.57–1.50 Ga. Younger suites intrude all terranes and vary in age from 1.52–0.92 Ga (Bingen *et al.* 2008; Petersson *et al*. 2015).

3.2 Sveconorwegian rocks

There are several models of the evolution for the Sveconorwegian orogeny. Slagstad *et al*. (2013) argue for a long lived accretionary margin with periods of extension and compression instead of a continent-continent collision, as the more accepted model imply. A four phase model for the Sveconorwegian, with different metamorphic stages, major and minor orogenic events is suggested by Bingen *et al*. (2008). It's divided into the Arendal phase, 1140–1080 Ma, the Agder phase, 1050–980 Ma, the Falkenberg phase, 980–970 Ma and the Dalane phase, 970–900 Ma (Bingen *et al*. 2008). The Arendal phase is an early collision stage and is characterized by high-grade metamorphism. The collision is between the Telemarkian and the Idefjorden terrane resulting in the forming of several crustal wedges (Ebbing *et al*. 2005; Bingen *et al*. 2008). The Agder phase is the main orogenic event with a continent-continent collision between Fennoscandia and what is thought to be Amazonia (Bingen *et al*. 2008). During the last stage crustal thickening, deformation, metamorphism and magmatism are recorded in the Idefjorden and Telemarkian terranes (Bingen *et al*. 2008). The Falkenberg stage also includes high grade metamorphism together with crustal thickening further in land in the Eastern segment (Fig. 1). Eclogite relics are found due to the burial of the segment to 50 km depth. In this stage the Idefjorden and Telemarkian terranes were thrusted on to the Eastern segment (Park *et al*. 1991; Bingen *et al*. 2008). The Dalane phase is the last stage of the orogeny and is interpret as a relaxation and gravitational collapse. The crustal thinning is driven by extension rather than erosion. The southern part of the Eastern segment and The Rogaland province in the Telemarkian terrane were exhumed to upper crustal levels (Bingen *et al*. 2008).

Rocks that are affected by the Sveconorwegian orogeny are exposed on the west coast of Sweden, and delimited by the Sveconorwegian Frontal Deformation Zone and the Protogin Zone in the east (Fig. 1). The rocks are divided in to the Eastern segment and the Idefjorden terrane (Åhäll *et al*. 1998; Åhäll & Connelly 2008; Petersson *et al*. 2015). The Eastern segment is made up of metamorphosed granites, syenites and later plutons ranging in age from 1.74–0.96 Ga (Johansson *et al*. 1993; Söderlund *et al*. 1999; Möller *et al.* 2007; Petersson *et al*. 2015 with sources within). Älgön intruded into the SLM (Fig. 1A) within the Idefjorden terrane, (Årebäck 1995).

3.3 Late Sveconorwegian intrusions

3.3.1 Rogaland anorthosite province

As part of the Anorthosite-Mangerite-Charnockite (AMC) suite in the Rogaland province, SW Norway, there are three massif-type anorthosite units; the Egersund-Ogna, Håland-Helleren and Åna-Sira (Schärer *et al*. 1996; Duchesne 1999; Bolle *et al*. 2003; Charlier *et al*. 2010; Vander Auwera *et al*. 2011). The units are all similar to the Hakefjorden Complex in several aspects, both in age and rock units. They all have a norite ma-

trix with Fe/Ti oxides. One of the most important ilmenite deposits in the world, the Tellnes deposit is found here (Duchesnes 1999).

Comparing the Norwegian anorthosite complexes, the grain size and foliation patterns are factors separating the units from each other (Schärer *et al*. 1996). They all contain HAOM and plagioclase megacrysts, typical for massif-type anorthosite, and they are all dated to around 930 Ma (Schärer *et al*. 1996; Duchesne 1999; Bolle *et al*. 2003; Charlier *et al*. 2010). Two pulses of post collisional magmatic suits have been dated in the area, the first and main pulse to 933–929 and the second to 920–916 Ma. The origin for the magmas is thought to be the lower crust. The massif-type anorthosite units formed in the first and main magmatic event (Vander Auwera *et al*. 2011).

3.3.2 Bohus granite

This composite granite complex is located along the Swedish west coast and can be found in an area of roughly 2000km in both Sweden and Norway (Fig 1A Eliasson *et al*. 2003). It consists of several intrusive stages and granite varieties that range from porphyritic to even grained grey to red granites (Eliasson *et al*. 2003). The c. 920 Ma Bohus granite is broadly synchronous with the Hakefjorden Complex (Eliasson & Schöberg, 1991).

3.3.3 Vinga intrusion

The Vinga intrusion (Fig. 1A) is dated to 951 ±7 Ma (Årebäck *et al.* 2008), making it significantly older than the Hakefjorden Complex with similar well-preserved igneous textures (Årebäck *et al.* 2008). The Vinga intrusion is a plagioclase porphyric granite to quartz monzonorite that intruded into the SLM, but with no visible contacts to host rock (Årebäck *et al.* 2008). Thermobarometry yield temperatures around 1000°C and 5–6 kbar for the source melting. The emplacement depth was decided to <7 km at <2 kbar and temperatures to 750–800°C (Årebäck *et al.* 2008).

3.3.4 Gothenburg dykes

The Gothenburg dykes (Fig. 1A) are made up of W-NW trending roughly 25 m wide monzogabbroic dykes and are rich in Ti, K and P (Hellström *et al*. 2004; Årebäck *et al*. 2008). Hellström *et al*. (2004) have dated the dykes to 935 ±2.9 Ma. The dykes are discordant to the ductile structures of the host rock and show no signs of metamorphism. Only secondary affect caused by hydrothermal fluids is seen in mineral alteration (Hellström *et al*. 2004).

4 Hakefjorden Complex

The complex only crops out on Älgön and Brattön and consists of anorthosite block in a norite matrix together with some minor units of monzonorite and the IRL. A map over the island and its rock units are presented in figure 2. The Hakefjorden Complex is a post Sveconorwegian intrusion dated to 916 ±10 Ma (Scherstén *et al*. 2000) cutting the metamorphic fabric of the SLM, which surrounds the intrusion (Fig. 2; Årebäck 1995; Årebäck & Andersson 2002). The contact aureole reached anatectic conditions as granitic veins and metamorphic minerals are found in the metasediments (Fig. 2) (Årebäck 1995; Årebäck & Andersson 2002). Årebäck and Andersson (2002) determined the P/T conditions based on peak metamorphic mineral assemblages, to 890°–1015° C and 3,7–6,4 kbar. An intrusion depth was estimated to 21–22 km corresponding to low-P ultra-high temperature granulite facies conditions.

Årebäck (1995) proposed a polybaric crystallization history. The early forming anorthosite accumulating at the top of the magma chamber and then rise adiabaticly to a lower crustal level due to gravitational instability (Årebäck 1995; Årebäck & Stigh 1997). This is in line with the most accepted model for massif-type anorthosite emplacement (Duchesnes *et al*. 1999; Vander Auwera *et al*. 2000; Markl & Höhndorf 2003; Vander Auwera *et al*. 2011; Bybee *et al*. 2014; Chen *et al*. 2015).

Årebäck (1995) state that the plagioclase megacrysts represent parts of the anorthosite that broke of, and continued to grow separate from the anorthosite. Investigations of trace and major elements have been made to decide origin (Årebäck 1995; Årebäck & Stigh 1997, 2000; Årebäck & Andersson 2002).

Årebäck (1995) proposed the mafic enclave to be a remnant of the parental magma, giving an idea of the origin for the intrusion. The monzonorite was classified as a differentiation from the norite together with contamination from the host rock (Årebäck 1995). Theories about the formation and emplacement of the IRL are not discussed in further detail and remain an uncertain part of the evolution of the Hakefjorden Complex.

5 Methods

5.1 Field work

The field work was planned and carried out during mid-September 2014. The island is E-W trending and a topographic high in the landscape compared to other surrounding islands (Fig. 5). The IRL is only found on. Steep walls together with vegetation covering most outcrops made the field work difficult. Contacts between rock units were mapped together with mineral composition, structures and textures. Samples of all rock types were collected for further investigation (appendix 1).

5.2 Laboratory work

Rock samples were crushed by hand and then grinded to powder by a mill for whole rock analysis. The powders were sent to Acme Labs in Canada, for a total whole rock characterization of both major and trace elements. Thin sections were made at the Geological Institute Slovak Academy of Sciences. The thin sections were investigated in a polarization light microscope, for petrographic description. They were also

Fig. 5. Two pictures showing the field area. The anorthosite can be seen as light grey in the pictures, indicated by the arrows in the darker norite matrix. A) Taken standing on an anorthosite fragment on the west side of the island. B) Shows the steep walls of the intrusion to the contact and the host rock and anorthosite block.

studied under a Hitachi 3400N Scanning electron microscope (SEM) equipped with an Oxford EDS system and a Gatan Mini-CL system in more detail. One inch mounts were made by hand and then looked at in the same SEM as mentioned above as well as in MC-ICP-MS, which is described more detailed below. The igneous petrology software, Igpet was used to model and create diagrams for rocks and their mineral composition.

5.2.1 LA-MC-ICP-MS

In situ Sr-isotope analyses of plagioclase in the one inch mounts were performed by Laser ablation MC-ICP-MS using a Nu Plasma HR multi-collector inductively coupled plasma mass spectrometer (MC-ICP-MS) and a Photon Machine Analyte G2 laser microprobe at the Geological Survey of Finland in Espoo. Samples were ablated in He gas (gas flows = 0.4 and 0.1 l/min) within a HelEx ablation cell (Müller *et al.* 2009). Plagioclase megacrysts, anorthosite and matrix crystals were analyzed. All analyses were made in static ablation mode using the following parameters; beam diameter: 200 µm; pulse frequency: 10 Hz and beam energy density: 3.5 J/cm2. The MC-ICP-MS was equipped with 9 Faraday detectors and amplifiers with 1011 Ω resistors. During ablation data was collected in static mode (^{84}Sr-Kr, ^{85}Rb, ^{86}Sr-Kr, ^{87}Rb-Sr, ^{88}Sr). Measured isotope ratios were corrected for instrument fractionation using an exponential law and a ^{86}Sr/^{88}Sr value of 0.1194. The isobaric interference of ^{87}Rb on ^{87}Sr was monitored and corrected using the ^{85}Rb ion signal and a value of 0.38571 for the ^{87}Rb/^{85}Rb ratio. The isobaric interference of ^{86}Kr on ^{86}Sr was corrected using a 30s background measurement, preceding every ablation. The average total Sr signal obtained for plagioclase samples was 0.4 V. Under these conditions, 120 s of ablation are needed to obtain an internal precision of ≤ ±0.00005 (1s). A value for the decay constant of ^{87}Rb of 1.393×10^{-11} y^{-1} has been used in all calculations (Nebel *et al*. 2011). The accuracy of the laser ablation protocol was verified throughout the day of measurement by repeated analysis of an in-house plagioclase standard from a megacryst of the Cameroon volcanic chain (sample Mir a, Rankenburg *et al.* 2004). The laser ablation parameters were the same on the samples and the standards. During the course of this study, the average ^{87}Sr/^{86}Sr value obtained was 0.70311 ±0.00005 (2s, n=26), in line with the TIMS value of 0.70311 ± 0.0001 (2s, Rankenburg *et al.* 2004). The analytical result of the in-house standard range from 0.70303 to 0.70321, similar to the reference value. The initial ^{87}Sr/^{86}Sr is calculated using an age of 900 Ma. Full results are given in appendix 2.

6 Results

The SEM results show that the majority of the plagioclase has a labradoritic composition, with some going to more andesine and some to more bytwonite (Fig. 6 and 7). A variation in An-content varies between the different rock units as well as the different kinds of plagioclase (Fig. 6 and 7). The Sr-isotope MC-ICP-MS results show that the magma is homogenous, with little variation in the Sr-isotope content (Fig. 8 and 9). The Sr-analysis are not done in the exact same spot as the An-analysis but they are correlated to represent the same area in the plagioclase, so it should not affect the results. The full results from the SEM and the MC-ICP -MS are found the appendix 2 and 3 and the average An content in table 1.

For more detail on the oxides and their textures see Kullberg (2015).

6.1 Field relations

The intrusion is exposed in the central parts of the island, also corresponding to the topographic high and site of investigation. SLM is found in the topographic low parts of the island on the north and south sides. Migmatites, pegmatites and contacts melts are found close to the contact. Plagioclase megacrysts are found in the norite and an altered norite rock on the south side of the island moving up in to the central parts of the island (Fig 2 and 10A). Anorthosite fragments are most common along the contact to the host rock and at the outermost parts of the island on the west side (Fig. 2). The fragments varies in size from dm to tens of m (Fig. 10B–C). In the center of the island the IRL is found (Årebäck 1995; Årebäck & Stigh 2000). The

IRL have the same mineralogy as the norite but with a higher concentration of Fe/Ti oxides (Fig. 10B–C and D–E). The IRL contains high amounts of ilmenite together with smaller amounts of magnetite and hematite. The IRL is different from the norite as it has flow structures, which is not visible in the norite to the same extent (Fig. 10F and 10A). The flow structures have different directions in the matrix and in the oxide concentration areas. This shows that the magma chamber had a dynamic environment, of complex currents (Fig. 10F and 10A). Årebäck (1995) classified a hybrid rock on Älgön with mafic enclaves and this is also found along the contact on the south side close to the megacrysts (Fig. 11A). The monzonorite found along the contact is thought to be formed by fractional crystallization together with contaminations by the host rock. The transition between the rock units is gradual.

Table 1. The average An-content for the rock units.

Rock	An-content
Sugary anorthosite in IRL	66.8
IRL matrix	66.3
Plagioclase snowflake	66.6
Grey inclusion	81.1
Norite matrix	60.0
Megacryst in norite	58.0
Plagioclase inclusions in oxide	69.0
Magnetic vein	65.3
Megacryst in altered norite	52.7
Matrix in altered norite	55.9
Megacryst in mafic enclave	50.5
Oxide concentration	61.0
Anorthosite	58.5
Mafic enclave plagioclase	61.7
Hybrid matrix	42.6
Sugary anorthosite in altered norite	57.3

6.2 Hakefjorden rock units

6.2.1 Anorthosite

The anorthosite consist of: plagioclase, orthopyroxene, clinopyroxene, ilmenite, magnetite zircon, apatite, baddeleyite

Blocks of almost 100% plagioclase with only minor amounts of interstitial phases are found in the norite and IRL. The block size varies from dm- to tens of m with varying grain size (Fig. 11E–F). The smaller sugary inclusions in the IRL together with the bigger blocks often have an enrichment of oxides around them (Fig. 10B–C). The size of these inclusions varies on a cm-dm scale. The An-content in the medium grained anorthosite lies around An_{58} while the sugary

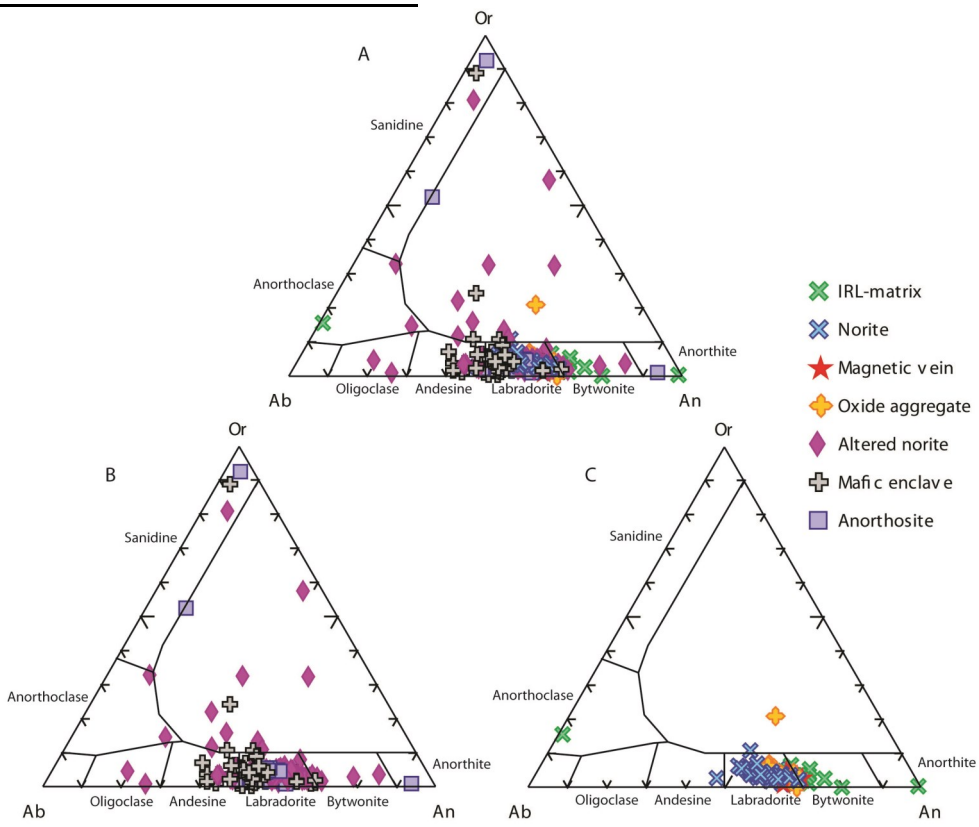

Fig. 6. Showing the SEM results as An-Ab-Or variation in the rock units. Some of the analysis gave strange values, plotting in the middle of the diagram, these are not taken into consideration during discussion. A) All of the analytical results for the rock units. B) The results for the altered norite, mafic enclave and anorthosite. C) The results for the IRL-matrix, norite, magnetic vein and oxide aggregate.

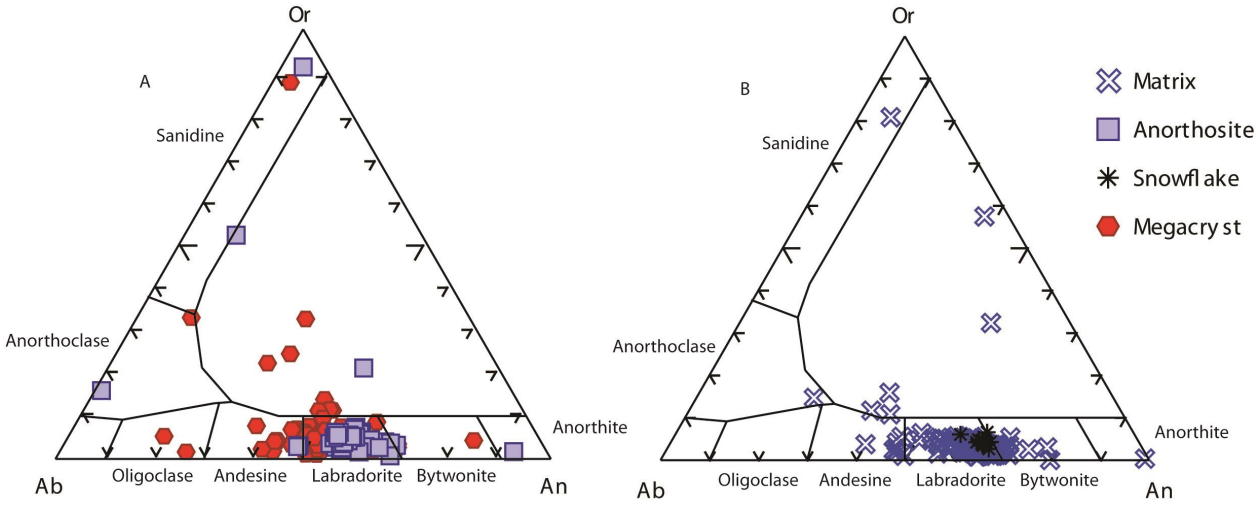

Fig. 7. Ternary diagrams showing the An-Ab-Or variation in the different types of plagioclase, results from the SEM. A) Shows the megacrysts, and anorthosites. B) Shows the matrix plagioclase, both needles and snowflakes.

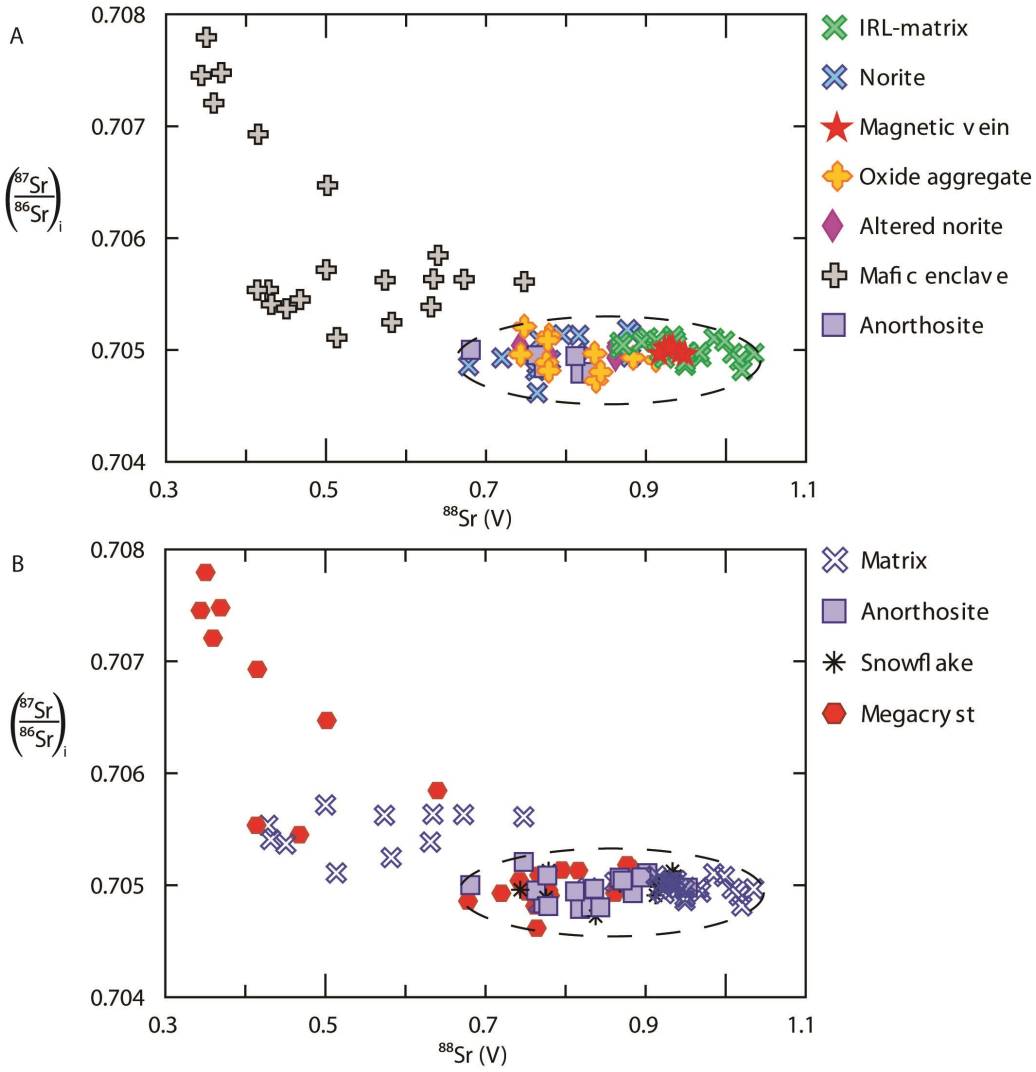

Fig. 8. Sr results, in the different rock units and the different types of plagioclase. A) The MC-ICP-MS results for the different rock units. The dashed line encircles the rock units of Hakefjorden Complex, showing how homogenous the magma is, only the mafic enclave have deviating values. B) The MC-ICP-MS results for the different plagioclase types. The dashed line encircles the main rock units of Älgön, only the mafic enclave lays above the rest.

anorthosite inclusions lie around $An_{57–67}$. Between grains and along fractures there is some alteration, and interstitial grains of orthopyroxene, apatite and oxides (Fig. 11D). Albite twinning is found both as straight lines and kinked. The contacts between grains are sharp even when altered. The needle texture of what might be antiperthite is found in the homogenous parts as in the megacrysts. They are common along grain boundaries and weak zones. In some samples the anorthosite have patchy zones to the host rock but not in the same way as seen in the megacrysts, as this looks more like post magma crystallization alteration (Fig. 11E). The Sr-isotope analysis showed that the initial $^{87}Sr/^{86}Sr$ is homogenous through the anorthosite with an average value at 0.70489 (Fig. 8 and 9; appendix 2).

6.2.2 IRL

The IRL consists of: plagioclase, orthopyroxene, clinopyroxene, ilmenite, magnetite zircon, apatite, baddeleyite, biotit

The distribution of the plagioclase in the matrix is usually isotropic and albite twinning is well developed, when visible. The plagioclase can also can occur as vein or enrichments (Fig. 10D). The IRL has the same mineralogy as the norite but is distinguished on the basis of high oxide concentrations and flow structures (Fig. 10B–C, D–F). The mineral contacts are sharp, but what looks to be reaction rims are seen in some samples. The plagioclase is found as: (I) subhedral to euhedral needles, (II) anhedral grains in small sugary anorthosite inclusions, (III) inclusions in other minerals or (IV) as snowflakes in the oxide rich areas.

Ilmenite dominates among the oxides on the island but magnetite is also found (Kullberg 2015). Compared to the other rock units of the intrusion, the oxides look very different in the IRL. They have a rounded shape compared to the rest where they are more angular or have a skeletal shape (Fig. 10D). For further detail see Kullberg (2015). Plagioclase is the other dominating phase in the IRL. In some areas a reaction rim can be found around the ilmenite in the contact to the plagioclase (Fig. 12A) found in both the matrix as subhedral needles and as sugary anorthosite inclusions (Fig. 12B and 10D). Snowflake grains occur in oxide rich areas in the IRL (Fig. 12C, 10E and 12D). Snowflakes are only found in the IRL and is either poikilitic grains, with oxide inclusions or as smaller individual grains and then the oxides are found as interstitial grains or smaller inclusions in the plagioclase (Fig. 12C). The snowflakes crystals are found in oxide aggregates. The average An-content in the snowflakes crystals is An_{67}, similar to the needles in the IRL matrix. The average An-content is An_{66} in the matrix including both needles and snowflake grains of plagioclase. The sugary anorthosite inclusions have similar values with An_{67}. The grains in the sugary anorthosite in the IRL have an anhedral shape, usually with higher An content than the other anorthosite (Fig. 12B). Where the plagioclase occurs as inclusions in the oxides they are in many cases spherical in shape, but also

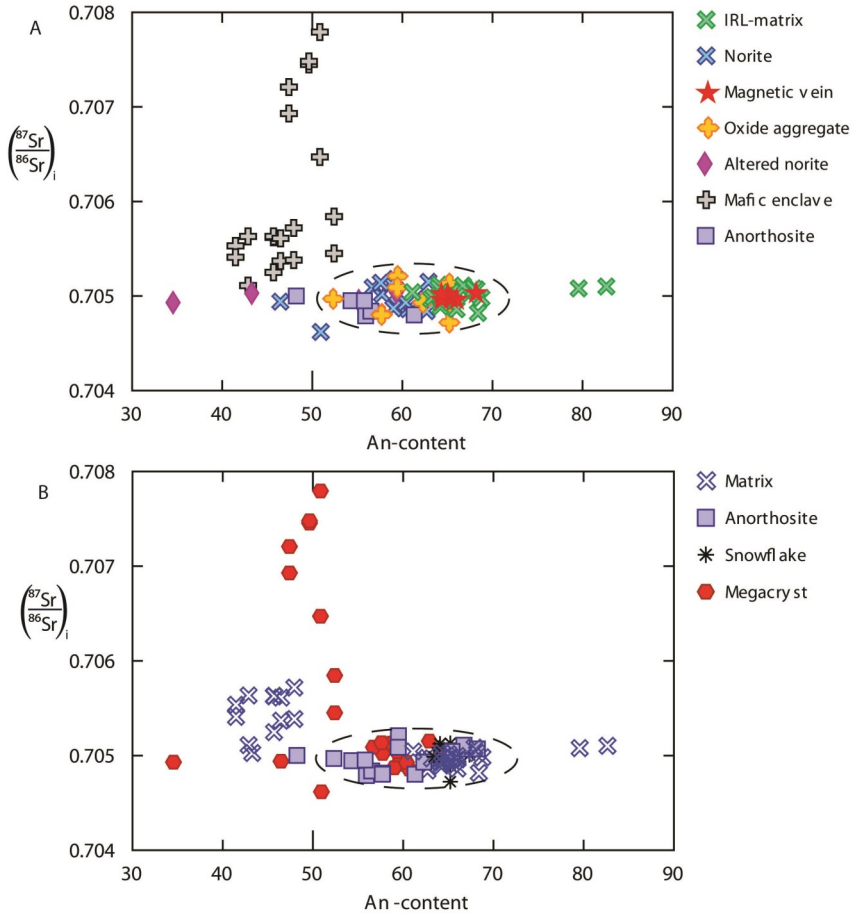

Fig. 9. The MC-ICP-MS results for the different rock units and the different types of plagioclase. A) The Sr plotted against the An-content of plagioclase in the different rock units. The dashed line encircles the main rock units of the complex, showing how homogenous the magma is, only the mafic enclave deviating from this trend. B) The Sr results plotted against the An-content of plagioclase in the different plagioclase types. The dashed line encircles the rock main units of Älgön, only the mafic enclave deviating from the rest.

Fig. 10. A) A band of megacrysts on the south side of the island, showing the dynamic magma chamber, not only in the IRL but in the norite as well. The pen in field pictures is 13.5 cm long. B) An anorthosite block in the IRL with an oxide aggregate around it. C) A smaller anorthosite fragment or plagioclase accumulation/sugary anorthosite in the IRL with an oxide aggregate around it, to illustrate that the phenomenon is visible on all scales. D) The picture were taken after examined in SEM, and carbon coated, can have affected the color. The picture is taken in XPL. An overview of the IRL matrix with the plagioclase needles, oxides and red biotite. E) an oxide aggregate with plagioclase snowflakes in the IRL. F) Showing the dynamic magma chamber in the IRL with flow structures, veins of oxides and dragged out anorthosite fragments.

found as more angular. The average An-content of these is An_{69}. Other inclusions found are oxide aggregates such as lens-like inclusions or enrichments around anorthosite inclusions (Fig. 10B–C) and undentified grey inclusions (Fig. 12D). The grey inclusions found in the IRL could not be sampled properly, so further investigation was hard to carry out. Plagioclase associated with the grey inclusions have a high

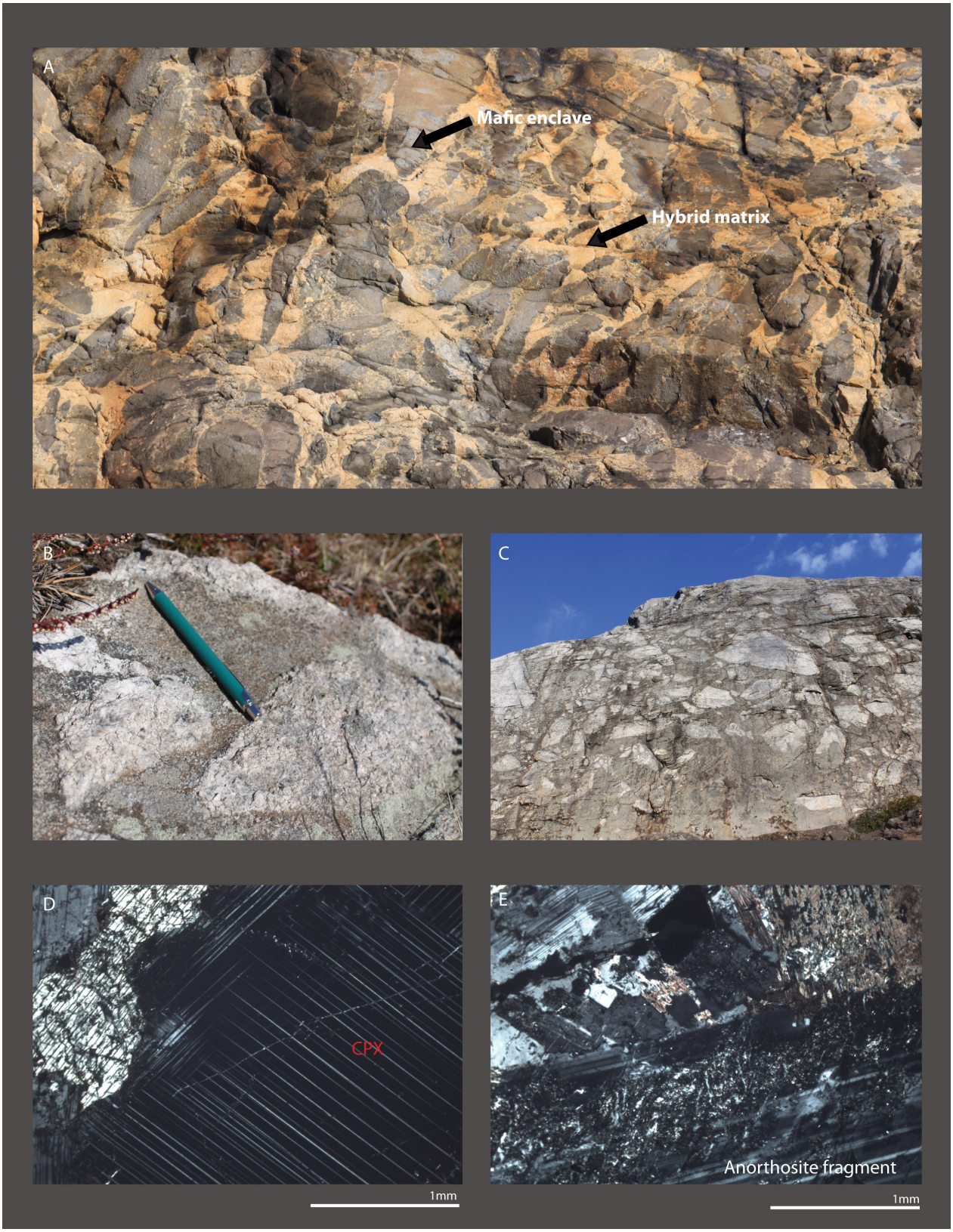

Fig. 11. A) The mafic enclave and its hybrid matrix showing assimilation in the enclave itself and the matrix. B) The pen in the picture is 13.5 cm long. The anorthosite in the IRL are angular and dm in size, a lot smaller than the blocks found on the west side of the island. C) The anorthosite block on the west side of the island varies in size on a tens of m scale. D) Taken in XPL showing the anorthosite and some of its interstitial phases. E) In the altered norite, showing the contact between a anorthosite fragment and the matrix, altered and the anorthosite is patchy.

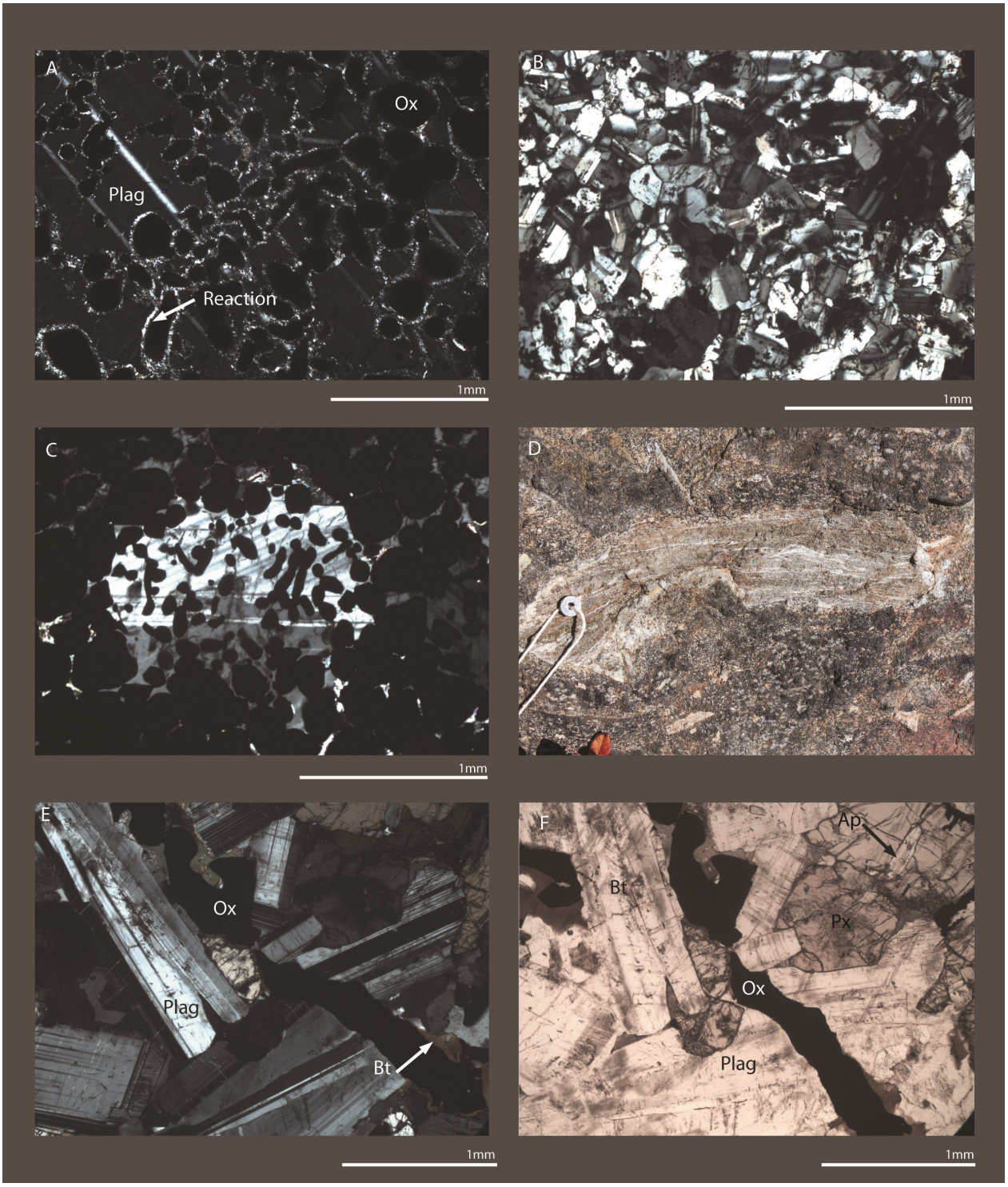

Fig. 12. Pictures were taken after carbon coated and examined in SEM. This can have affected the coloring. A) In XPL from the IRL, a reaction around the oxides in contact with plagioclase, rim is too small to be able to determine what it is. B) An sugary anorthosite inclusion from the IRL. C) A snowflake plagioclase from the IRL matrix. D) A grey inclusion in the IRL, with an oxide aggregate around it with plagioclase snowflakes. E) An overview of the norite matrix with plagioclase needles, oxides, pyroxene, red biotite and apatite. F) same view as E) but in instead to show some of the other mineral phases more clearly.

average An-content around An_{80}. The pyroxene is found as individual grains or as interstitial phases in oxide aggregate areas. Biotite has a more red color than usual and is found together with oxides like a halo around them (Fig. 10D). Late stage alteration is seen, same as in the other samples but not as far evolved.

The Sr-isotopic ratios vary, depending on the type of plagioclase. The variation is seen in the third to fifth decimal, when comparing the ratios. The $^{87}Sr/^{86}Sr$ varies between 0.07496–0.70509 in the different kinds of plagioclase in the IRL (Fig. 8 and 9; appendix 2).

6.2.3 Norite

The norite consist of: plagioclase, orthopyroxene, clinopyroxene, ilmenite, magnetite zircon, apatite, baddeleyite, biotit, quartz, k-feldspar

The norite is the main host rocks for the plagioclase megacrysts and anorthosite blocks (Fig. 11B–C, 13A). The contact between minerals is sharp all through the sample (Fig. 12E–F). The norite matrix around the megacrysts is isotropic with only later alteration; there are no reactions between the different mineral phases. The plagioclase in the norite matrix are found as subhedral needles with albite twinning and an average of An_{60}.

The megacrysts can be divided in to three different zones; the core, inner rim and outer rim (Fig. 13B). The cores are homogenous with no inclusions or patchy areas present as in the rims. The only texture seen is what looks to be antiperthite. What look to be secondary alteration and seritization is found along weak zones. The inner rims has a patchy look full of inclusions of orthopyroxene, clinopyroxene, apatite and Fe/Ti oxides (Fig. 13B). The outer rims again look like the homogenous cores of the megacrysts without patchy spots and inclusions (Fig. 13B).

In several samples the albite twinning continues from the core uninterrupted through the inner rims to the outer rims. In this case the inner rims is characterized by having inclusions without patchy appearance. If there are cracks or weaker areas in the megacryst the adjacent region to these are patchy and altered together with inclusions. All megacrysts show albite twinning, mostly straight but in some cases kinked, some even have more chessboard like twins, with smaller tartan patterns in between (Fig. 13C). The An-content in the megacrysts signs of oscillatory variation in some megacrysts (Fig. 14). The average An content in the megacrysts found in the norite is An58 The An-content varies from the core out to the rim in the megacryst (Fig. 14).

The biotite is often found in association with oxides as in the IRL, having a red color (Fig. 12E–F). Quartz is found as anhedral grains, same as the pyroxene. The pyroxene grains are interstitial (Fig. 12E–F). Both the ilmenite and the magnetite have an anhedral, sceletal shape, with spherical inclusions and exsolution lamella of different kinds (Kullberg 2015). The ilmenite have some hematite lamella while the magnetite have trellis lamella of ilmenite (Kullberg 2015) Apatite is found as euhedral to subhedral grains (Fig. 12F).

The Sr-isotopic ratios in the megacrysts and norite matrix all within the same span as the other rock units (Fig. 8 and 9; appendix 2).

6.2.4 Mafic enclave and hybrid matrix

The mafic enclave and hybrid matrix consists of: plagioclase, orthopyroxene, clinopyroxene, ilmenite, magnetite zircon, apatite, baddeleyite, biotit, quartz, k-feldspar, amphibole

Årebäck (1995) interpreted the hybrid rock with mafic enclaves, as a possible remnant of the parental magma for the intrusion (Fig. 11A). The enclaves are fine grained on the boarder to aphanitic, with a coarser matrix with roughly the same mineralogy. The mafic enclave contains plagioclase megacrysts. These megacrysts can as the ones in the norite be divided into zones; the core and rim. What look to be secondary

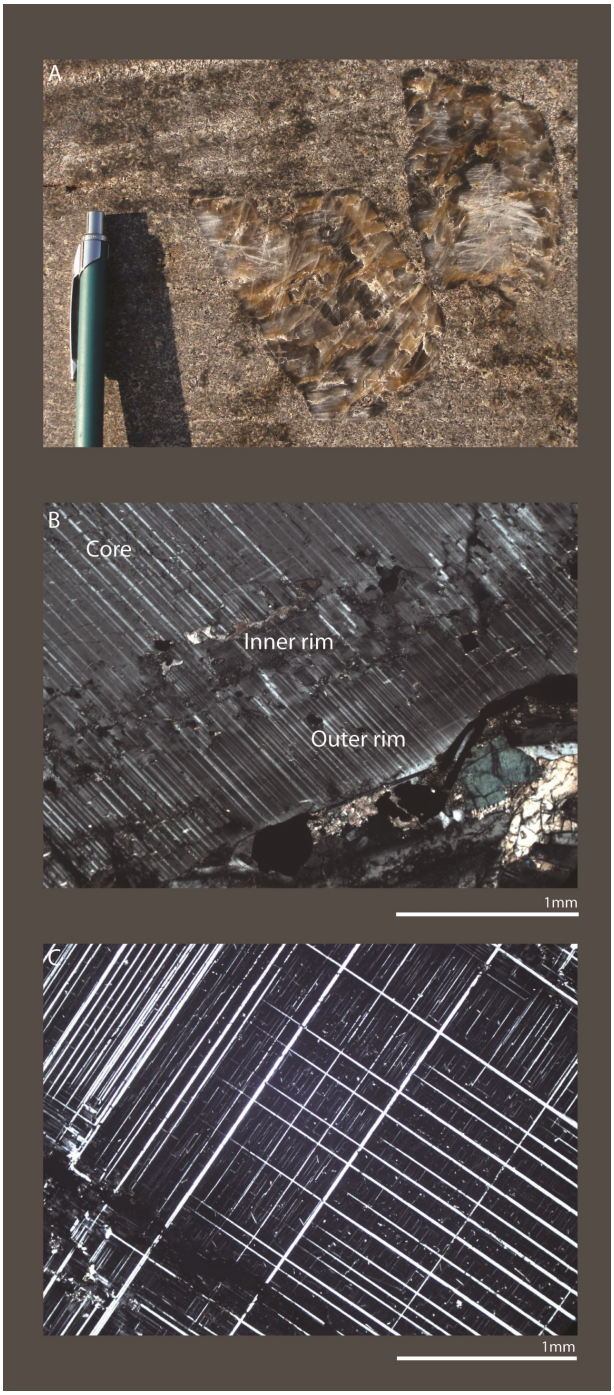

Fig. 13. The pen in field pictures is 13.5 cm long. A) Megacrysts in the norite matrix along the south side of the island. Pictures were taken after carbon coated and examined in SEM. This can have affected the coloring. All pictures are taken in (XPL). B) A plagioclase megacryst from the norite matrix, showing the core, inner and outer rim and the contact to the norite matrix. C) Showing the twinning in the megacryst, chess board pattern with smaller in-between.

alteration and seritization is found along weak zones.

In several samples the albite twinning continues from the core uninterrupted through the inner rims to the outer rims. In this case the inner rim is characterized by having inclusions without patchy appearance. If there are cracks or weaker areas in the megacryst the adjacent region to these are patchy and altered together with inclusions. The An-content in the megacrysts varies between the rock units, with signs of oscillatory variation in some megacrysts (Fig. 15). The megacrysts in the mafic enclave have a lower average of $An_{50–53}$ with big internal variations compared to the megacrysts in the norite. The An-content varies from the core out to the rim in the megacryst (Fig. 15). The contact between the mafic enclave and the hybrid matrix is sharp (Fig. 16A). Several different types of plagioclase megacrysts are found in the mafic enclave (Fig. 16B–E). There are those full of inclusions all through the grain (Fig. 16B), only in the center of the grain (Fig. 16C), in only the rim of the grain (Fig. 16D), or no inclusions at all (Fig. 16E). The inclusions found in the cores and rims are orthopyroxene, clinopyroxene, apatite and Fe/Ti oxides. The patchy look seen in the inner rim in the megacrysts in the norite is not found to the same extent here. The An-content varies depending on what type of plagioclase it is. The ones with no inclusions and full of inclusions both have an average $An_{48–49}$, the ones with only inclusions in the rims have an average $An_{51–52}$ and the ones with only inclusions in the centers have an average of An_{57}. The average in the hybrid matrix is An_{42} and in the mafic enclave looking at the megacrysts the average is An_{50}. In some of the plagioclase are so altered, that it's almost impossible to say what's still primary plagioclase (Fig. 16F). Alteration by late stage magmatic fluids, make it hard to get good analytical results.

The rock unit shows a different initial $^{87}Sr/^{86}Sr$ and variation than the rest of the rock units (Fig. 8 and 9). The An content is relatively low but with big internal variations between the enclave, the hybrid matrix and the different analytical points (appendix 3). The hybrid matrix has an average Sr-isotopic ratio of 0.70548 (Fig. 8 and 9). The mafic enclave megacryst has a greater variation, with zonation from core to rim (Fig. 15), with overall higher average initial $^{87}Sr/^{86}Sr$ than the other rock units (Fig. 8 and 9; Appendix 2).

6.2.5 Altered norite

The altered norite consists of: plagioclase, orthopyroxene, clinopyroxene, ilmenite, magnetite zircon, apatite, baddeleyite, biotit, quartz, k-feldspar, amphibole, chlorite

The grain size change between samples, but the mineralogy stays the same. Anorthosite fragments and plagioclase megacrysts are found in several of the samples (Fig. 11E, 17A and B–C). The megacrysts does not look more altered than the megacrysts found in the norite (Fig. 17B–C), but the average An values is lower (appendix 3). They look the same as previously described, no reaction rims or other textures . The

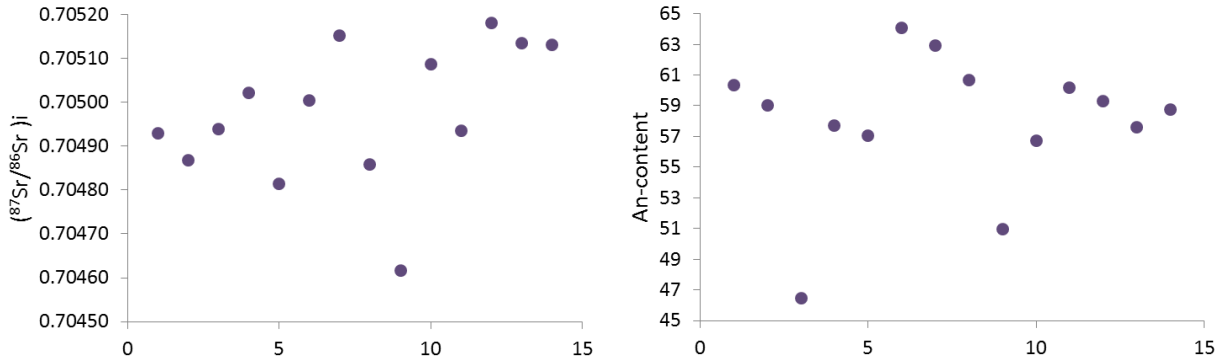

Fig. 14. Show a plagioclase megacryst in the norite, from the core to the rim. The Sr ratio variation to the left and An variation to the right.

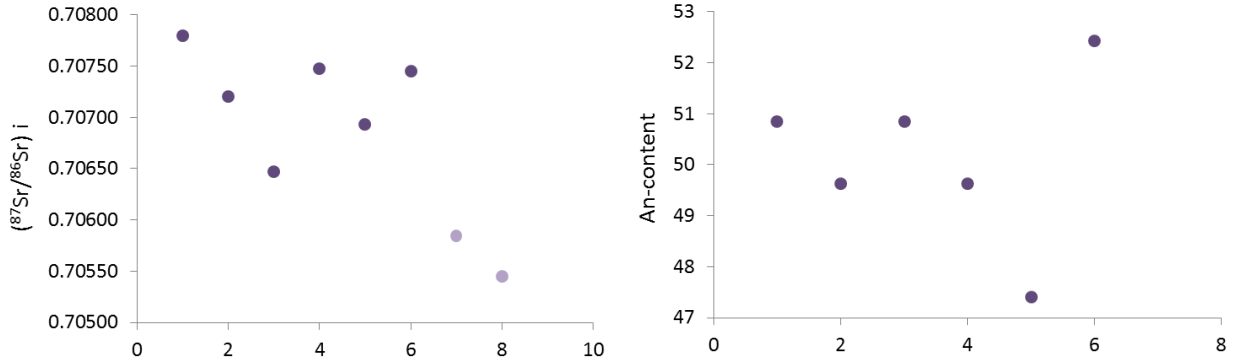

Fig. 15. Show a plagioclase megacryst in the mafic enclave, from the core to the rim. The Sr ratio variation to the left, where the light purple dots are in the rim and the dark in the core and out to the rim. To the right the An-content is illustrated.

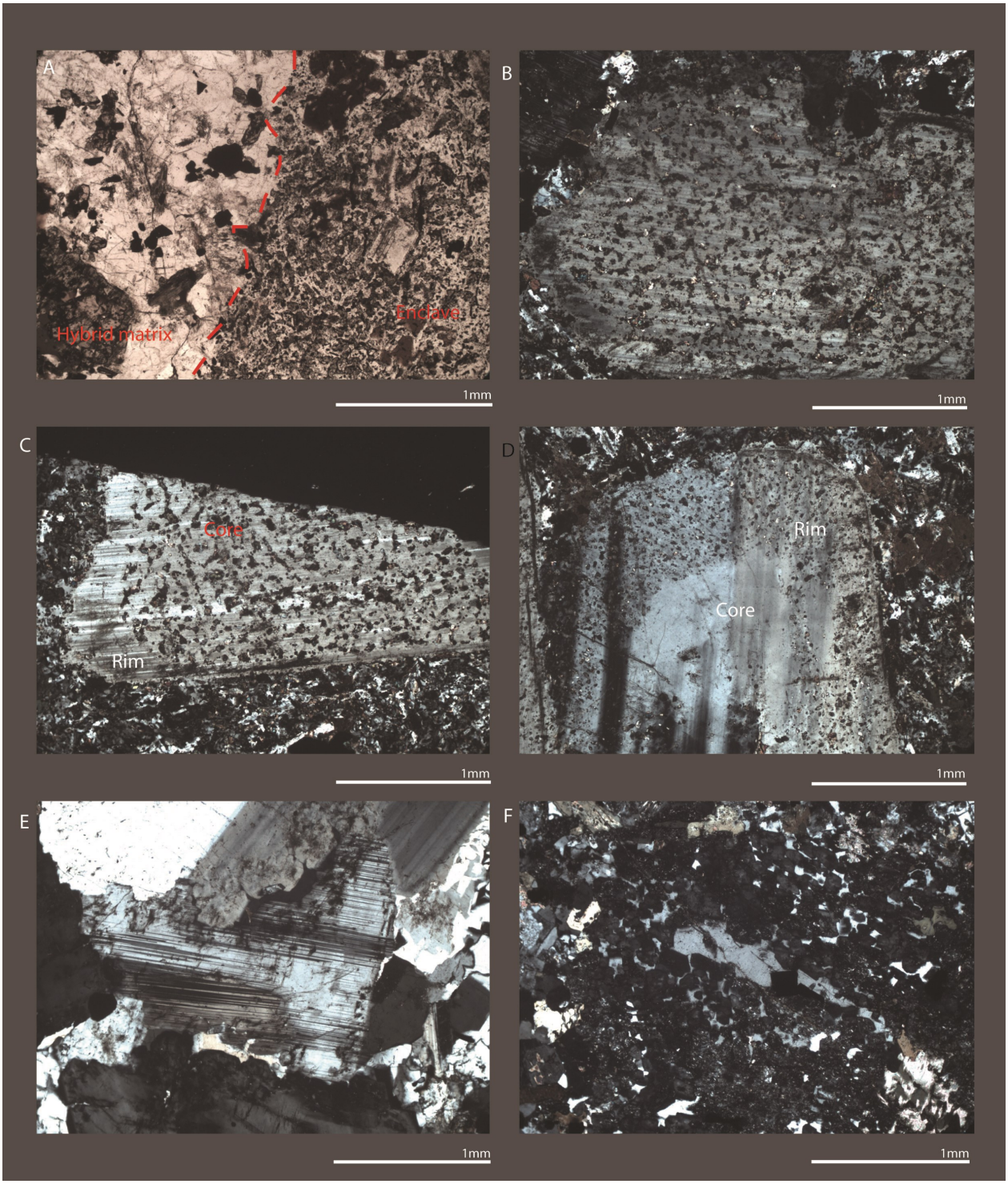

Fig. 16. A) Taken in ppl showing the mafic enclave and its hybrid matrix contact, can see clear variation in grain size between the mafic enclave and the hybrid matrix. B) On of the several different types of plagioclase megacrysts in the mafic enclave, having inclusions and a muchy look all throughout the megacryst in XPL. C) A second type of megacryst in the mafic enclave, this with only inclusions and a patch look in the center of the megacryst in XPL. D) A third kind of plagioclase megacryst in the mafic enclave, with only inclusions in the rim and not the core of the megacryst. In XPL. E) The last kind of plagioclase megacryst in the enclave have no inclusions at all or any patchy look. In XPL. F) Disequilibrium in the hybrid matrix to the mafic enclave.

ilmenite has a skeletal shape (Fig. 17D). Some late alteration has started to transform the pyroxene to amphibole. Some of the ilmenite grains in the samples contain titanite, also from later alteration (Kullberg 2015). The plagioclase needles in the matrix are also altered by late stage magmatic fluids (Fig. 11E 9 D and 17D–E).

The mineral contacts are sharp, no reactions rims are visible. Albite twinning can be seen in places when the alteration doesn't goes all through the grain. Symplectites/granophyric textures are seen in some of the samples (Fig. 17E). Årebäck (1995) described similar textures of K-feldspar and quartz in monzonorite, these could be similar to those. The An-content in the rock unit varies between the different samples and between matrix and megacryst but the average in the matrix is An_{56} and in the megacrysts it's An_{52} (Fig. 6 and 7; appendix 3). Fragments of sugary anorthosite in the altered norite have an average of An_{57}. Few values came out of the Sr-analysis, and only one sample was analyzed. But the average Sr-isotopic ratios for the megacryst are 0.70499. Only one point could be analyzed in the matrix, with a value of 0.70503 (Fig. 8, 9; appendix 2).

6.2.6 Monzonorite

The monzonorite consists of: plagioclase, orthopyroxene, clinopyroxene, ilmenite, magnetite zircon, apatite, baddeleyite, biotit, quartz, k-feldspar, amphibole

High grade of alteration by late stage magmatic fluids in the sample made it difficult to deduce which phases that represent primary plagioclase (Fig. 17F). Plagioclase is a minor phase in the monzonorite. The high grade of alteration together in the rock led to that no usable data was obtained. Zircon grains are found in all the samples but in this rock they are bigger and more numerous (Fig. 17F). The oxides are usually found together with pyroxene, biotite or amphiboles. The rock is altered, but when visible the contacts between minerals are sharp, with no visible reaction rims. No Sr-analysis was done on this rock unit.

6.2.7 SLM

The SLM consists of: quartz, muscovite, biotite, zircon

Host rock for the intrusions is a foliated fine-grained gneiss made up of quartz, muscovite, biotite with minor amounts of zircon and apatite. There is little secondary alteration, with sharp contacts between the minerals. Quartz is found in the ground mass but also as veins. The initial $^{87}Sr/^{86}Sr$ for the SLM is a lot higher than for the rest of the island rocks shown both in this study and regional values from previous investigations (Daly *et al*. 1979; table 2).

6.3 Geochemical data

The full results from the whole rock analysis are presented in appendix 4. A big variation in both major and trace elements can be seen between the different rock units (appendix 4). The An values based on the whole rock results is not represent table since the rock units contain more minerals which incorporate Ca than plagioclase, such as clinopyroxene and apatite. But the An values show good correlation with the SEM results in that high An values are found in the IRL having $An_{64–68}$ while the anorthosite has An_{56} same as the mafic enclave (appendix 4). For details on the trace elements analysis and more detail concerning the whole rock results and the Fe/Ti oxides see Kullberg (2015).

6.4 Sr-isotopes

The laser ablation was performed to examine the Sr-isotope ratios and their variation between plagioclase in different rocks. The analytical spots are shown in figure 18. The full results are presented in appendix 2. The $^{87}Sr/^{86}Sr$ between the rock units do not vary signif-

Table 2. Regional Sr-ratios from an augen gneiss in the SLM (Daly *et al.* 1979).

$^{87}Rb/^{86}Sr$	$^{87}Sr/^{86}Sr$ t=0	t (Ma)	$^{87}Sr/^{86}Sr$ t=t
5.805	0.83	920	0.7537
3.663	0.78317	920	0.7350
4.005	0.78991	920	0.7372
7.275	0.85456	920	0.7589
9.416	0.89409	920	0.7703
5.132	0.81566	920	0.7482
4.45	0.8024	920	0.7439
4.308	0.79984	920	0.7432

icantly (Fig. 8 and 9). The only rock that does not have the same Sr-signature as the rest is the mafic enclave, with higher values than the rest (Fig. 8 and 9). The enclave does not show homogenous Sr-isotopic ratio distribution within the sample. One megacryst in the enclave has a lot higher $^{87}Sr/^{86}Sr$ in the core and lower in the rim (Fig. 19), while in the hybrid matrix all plagioclase Sr-isotopic ratios are as the rim of the megacryst in the enclave (Fig. 19).

7 Discussion

It has to be taken in to account that the results, due to problems with the SEM, have big internal variation and that many analytical points lie a bit from the optimal 100% weight percentage wanted for best results. The SEM measurers the amounts of inaccurately, so the total either falls above or under the optimal 100%. This means that incorrect values for the elements in the minerals are recorded. All the results are used as the An values are not affected by normalization, as the internal relation between Na, Ca and K stays the same.

The sugary inclusions are probably not related to the anorthosite block but are instead interpreted as accumulations of plagioclase due to the chamber current as the IRL started to crystallize. The plagioclase snowflakes are interpreted as an early stage of plagioclase accumulation that later evolve to become the sugary anorthosite. This is supported by that fact that the An content of the snowflakes are not so far from the sugary inclusions.

The plagioclase megacrysts within all rock units, excluding the mafic enclave show very homogenous An and initial $^{87}Sr/^{86}Sr$ (Fig. 6–9). Since there is no clear zonation but only some oscillatory variations

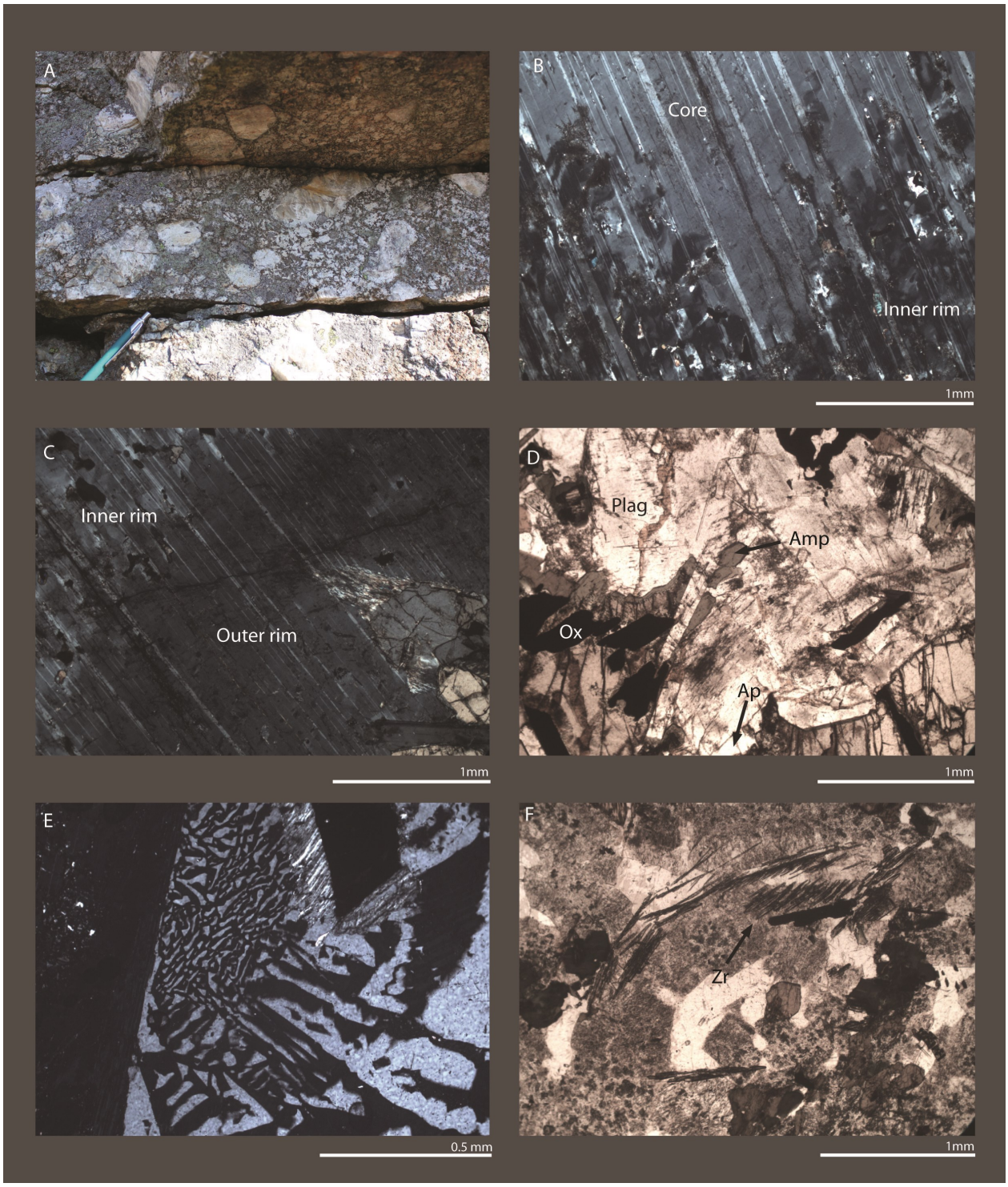

Fig. 17. The pen in field pictures is 13.5 cm long. A) Megacrysts further up on the island in the altered norite. B) Showing the core and inner rim in a plagioclase megacryst from the altered norite, similar appearance as the megacrysts from the norite but with a larger patchy zone. C) Showing the inner rim and outer rim in a plagioclase megacryst from the altered norite. D) showing the altered norite matrix in, to show the mineral phases more clearly. E) The symplectite/granulation texture of the altered norite. F) The monzonorite matrix with large zircons, marked by arrows. The alteration can also be seen, affecting several of the phases in the sample.

(Fig. 14, 15), the conclusion of a homogenous magma over a long time can be drawn. (Fig. 6–9). The three zones seen in the megacrysts are interpreted to have formed during emplacement. When the crystal mush traveled up after forming the megacrysts they were in disequilibrium with the melt, gave rise to the patchy look. When finally at place in the crust they continued to grow normally outside of the patchy inner rim.

Reaction rims between oxides and plagioclase are visible in some samples. The rims looks like they are

mantling the oxides but the phase is too fine grained too decide what it's made of (Fig. 12A).

Currents in the magma chamber are interpreted to be responsible for the anorthosite block distribution, as well as the plagioclase megacryst (seen in previous pictures). This is also the reason the IRL is found in the middle of the intrusion (Kullberg 2015).

The results of Kullberg (2015) indicate that the intrusion crystallized from inside out and not the normal cooling from the edge to the center. Kullberg (2015) also show that more enriched rocks are found on the edge of the intrusion, as the monzonorite.

7.1 Sr-isotopes and An content

Both Sr-isotopes and the An-content indicate a very homogenous magma. Only the mafic enclave show a more radiogenic signature (Fig. 8 and 9). The results show that little contamination or mixing of magmas have occurred. Fractional crystallization is the dominating process affecting the plagioclase chemistry. Pressure affects the chemistry of plagioclase as well but in a smaller degree, which will be explained in detail below. The pressure affect can possibly be seen in An variation within the same rock unit but between the units the An variation is too large to be explained by difference in pressure. Other factor that can affect the chemistry is temperature and H_2O content of the magma, but they are minor factors compared to fractional crystallization. A combination between several of the minor factors as temperature and if any other calcic incorporating phases are crystallization, as apatite or clinopyroxene the effect will be increased.

Bowen's reaction series show that Ca-rich plagioclase will be the first plagioclase to crystallize and then move over to more Na-rich plagioclase as the crystallization proceeds, unless pressure decreases. This concludes that the IRL-matrix together with magnetic vein and oxide aggregate was first to crystallize (Fig. 6 and 7). After the IRL started the norite, the altered norite, the megacrysts, anorthosite and lastly the mafic enclave. The sequence is based on the An content together with the results of Kullberg (2015). The lower An values of mafic enclave might also be related to the fact that it's mixed with other rock units, showing a more crustal signature (Fig. 6). These results correlate with the AFC-modelling and and oxide analysis results of Kullbergs (2015).

The megacrysts generally have a more andesitic composition than the matrix (Fig. 6 and 7). Utsuninski *et al*. (2014) showed that lower An content can be related to magma decompression, the size of the plagioclase megacrysts either indicate that they crystallized over a longer time, or quick transport of elements to exhilarate growth speed and get big crystals in a short time. The decompression phase have to be long for them to have time to grow to that size. Together with other results (Blundy & Wood 1991; Vander Auwera *et al*. 2000) the pressure effect on the composition of plagioclase when crystallizing is not a major factor, but can contribute to the An variation (Panjasawatwong *et al*. 1995). Based on these studies the crystallization of plagioclase megacrysts and anorthosite on Älgön is different from the matrix plagioclase and the conclusion that they did not all start crystallizing at the same time can be taken (Fig. 6 and 7). The An-content in the matrix plagioclase varies between $An_{60–70}$, $An_{50–60}$ in the anorthosite and $An_{43–58}$ in the megacrysts depending on what matrix they are found in (table 1). In the norite the An-content of the megacrysts lie around An_{60} while it varies between $An_{46–52}$ in the altered norite indicating fractional crystallization, differentiation and pressure variation in the rock units during the crystallization. The monzonorite, mafic enclave and altered norite are to altered to be sure about the results, since not many unaltered domains are appropriate for analysis. This is especially true for the monzonorite. But they still give a hint in what direction the values tend to go.

In the mafic enclave the initial $^{87}Sr/^{86}Sr$ variation shows a deviating pattern compared to the other samples. In the core of the megacrysts the Sr-values are high (Fig. 8 and 9) and within plagioclase grains in the hybrid matrix and the rim of the megacrysts, the Sr amount is lower (Fig. 19). The Sr concentration, represented here by the Sr (V) vary systematically within the plagioclase from core to rim.

The other rocks have even lower Sr-isotopic ratio values. The rock units lie together in a cluster under the megacrysts of the mafic enclave and the hybrid matrix (Fig. 8 and 9).

The initial $^{87}Sr/^{86}Sr$ indicate little to no contamination from the SLM, only fractional crystallization trend seen as, horizontal distribution of values (Fig. 21). Contamination would have been visible as variation along the vertical axis, however this is only observed in analysis from the mafic enclave (Fig. 21). But this would be hard to explain with contamination, since the high values are found in the cores of megacrysts and not in the rim, indicating other source/ contaminated before the other rocks formed.

The higher Sr values in the cores compared to the rims in the mafic enclave shows that something have mixed. The main group of rocks lies in a cluster while the mafic enclave is mixing up towards more crustal signatures (Fig. 21). Horizontal distribution of the main group and the hybrid matrix group indicate fractional crystallization without contamination or influx of new magma with contrasting $^{87}Sr/^{86}Sr$. The main rocks would have started to form and then mixing generated the deviating patterns of the mafic enclaves deviating pattern. Then the hybrid matrix together with the rims of the megacrysts homogenized.

7.2 Hakefjorden Complex

Results in this study compared to previous work (Årebäck 1995; Årebäck & Stigh 1997 etc) do not agree in all aspects. Årebäck (1995) thought that the mafic enclave was a fractionated remnant of the parental magma for the complex but the variation in Sr-isotope ratios rejects this hypothesis (Fig. 8 and 9).

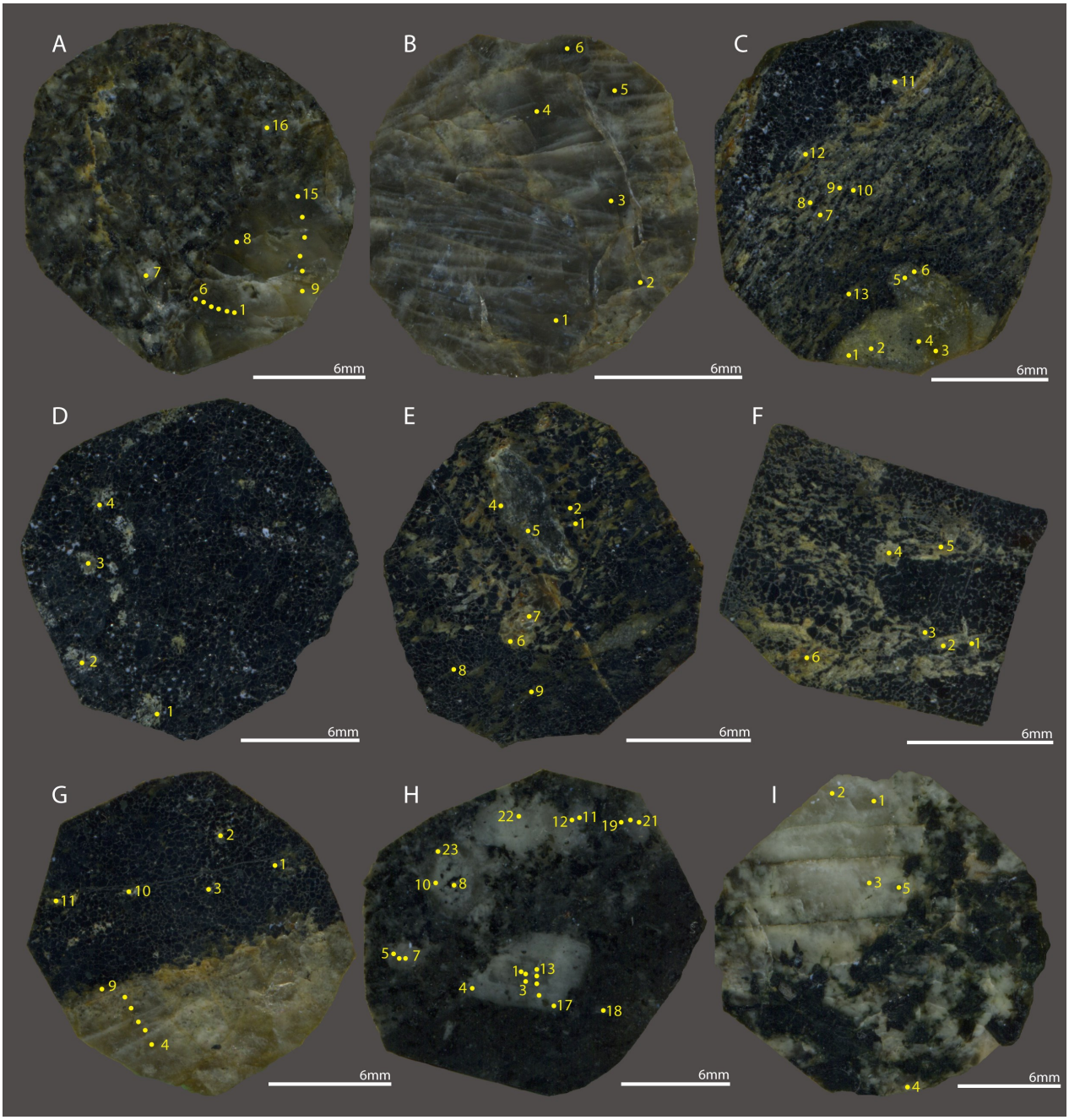

Fig. 18. Showing the analytical points for the MC-ICP-MS in the different mounts. The analytical points are marked in yellow and to identify the point in appendix 3 there is a number coupled to the point as well. A) The norite matrix with a plagioclase megacryst on the bottom right of the mount. B) The medium grained anorthosite. C) The IRL matrix with a sugary anorthosite inclusion on the bottom of the mount, and some plagioclase snowflakes D) Snowflake plagioclase in a oxide aggregate in the IRL. E) Showing the IRL-matrix with a grey inclusion and some plagioclase snowflakes. F) A magnetic vein with IRL matrix plagioclase needles. G) An oxide aggregate with a sugary anorthosite inclusion. H) The mafic enclave with the hybrid matrix. The plagioclase megacryst with irregular Sr-isotope values and An zonation is seen in the middle of the mount. I) An altered norite with a plagioclase megacryst in part of the mount. High grade of alteration made it was hard to get good analytical results.

The initial $^{87}Sr/^{86}Sr$ are too high, showing an enriched, crustal signature compared to the rest of the rock units. The examined megacrysts in the mafic enclave together with its hybrid matrix show different Sr-signals than the remaning units on Älgön (Fig. 8 and 9). This is the only rock on the island that is mixed, contaminated and possibly from another source (Fig. 21).

The chemistry and An-content of the plagioclase in the rock units is a lot more calcic than previously documented (Årebäck 1995; Årebäck & Stigh 1997). Årebäck & Stigh (1997) found that the plagioclase has a different An content in the matrix of the different rock units compared to the megacrysts or the anorthosite. The average values in the matrix $An_{54.2}$ and around An_{46} average in the megacrysts and anorthosite. The results from this study confirm that the An content

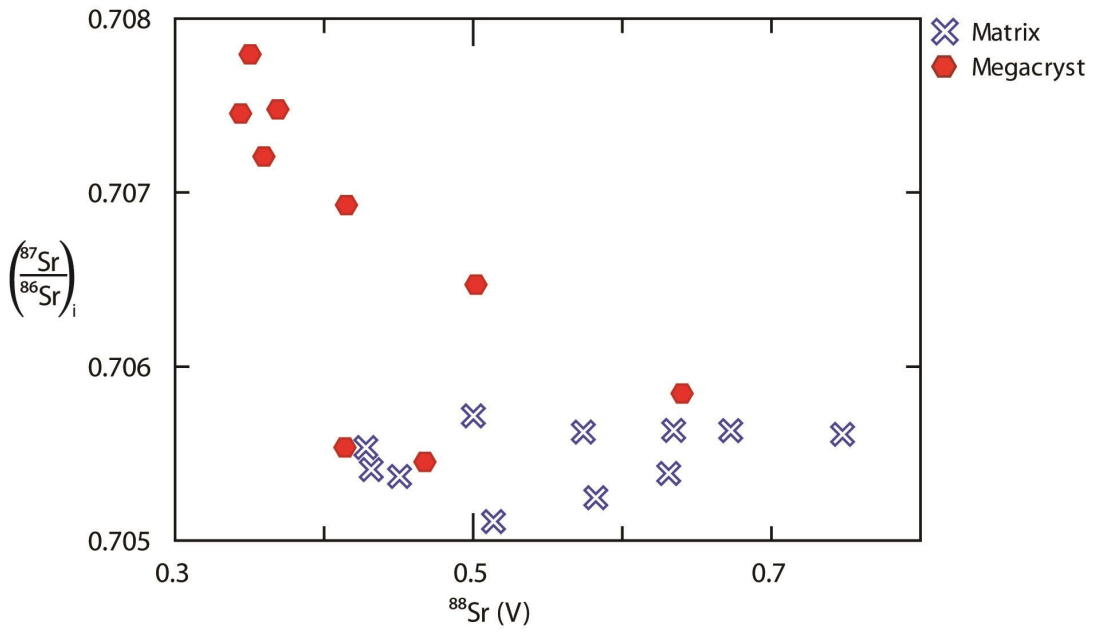

Fig. 19. The Sr results, only for the mafic enclave. Illustrates the different in hybrid matrix and megacryst in the mafic enclave. The three points in together with the matrix values represent the rim of the megacryst, while the point higher up is from the core gradually moving towards the rim.

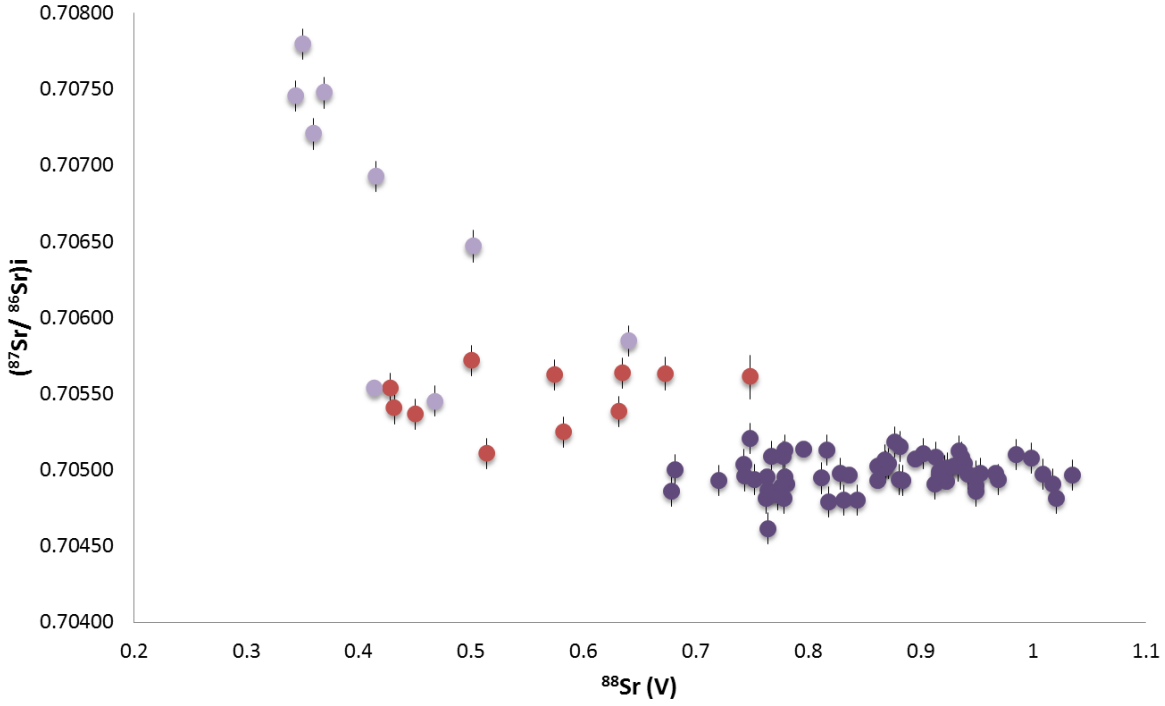

Fig. 20. Shows the Sr results from the MC-ICP-MS with error bars. The error on the analysis is in several point smaller that the marker itself. The light purple shows the megacryst in the mafic enclave, the red dots show the hybrid matrix plagioclase and the darker the main rock units.

varies between matrix, megacrysts as well as between different rocks units. The matrix in the norite has an average of An_{60}, the IRL An_{66} and the altered norite An_{56} (Table 1). The megacrysts in the separate rock units vary substantially between the different matrix and analytical point (Table 1). The megacrysts found in the norite have an average values of An_{58}, the altered norite yield's an average of An_{52} and the mafic enclave yield An_{50}. The anorthosite fluctuates from An_{57} to An_{68}, where the sugary anorthosite inclusions in the IRL have higher An-values than the anorthosite blocks (table 1). One norite samples together with the mafic enclave and hybrid matrix record the lowest values ranging from An_{39} to An_{46} with some outliers as

high as An_{68}.

Previous theories about emplacement and formation of the complex, having a polybaric crystallization and adiabatic rise, suggested by Årebäck (1995) seem likely to be accurate. Other theories of magma mixing, being part of the island evolution are not in line with the results from this study. This is based on the Sr ratios from the MC-ICP-MS (Fig. 8 and 9) as only the mafic enclave has deviating values indicating crustal contaminant (Fig. 21).

7.3 AFC assimilation and fractional crystallization

The results from this study together with the results of Kullberg (2015) suggest that there is little or local contamination from the host rock in the Hakefjorden rock units (Fig. 21). The mafic enclave is the only sample that trends toward more crustal signatures and mixing with another crustal source (Fig. 21) Panjasawatwong *et al*. (1995) showed that the Ca content in plagioclase is dependent on pressure, H_2O content, Ca# and Al# in the melt. Showing that the melt composition is responsible for the large change of An content, and not pressure variation. The highest An content in plagioclase is recorded in the IRL matrix, sugary inclusion and in relation to the grey inclusion. Together with the results of Kullbergs (2015) the IRL is interpreted to be the first phase to crystallize (Fig. 6 and 7).

Traces of contamination in the rocks are small, looking at the Sr-isotope ratios (Fig. 21). The initial $^{87}Sr/^{86}Sr$ ratios in the host rock might be the reason for the crustal signature in the mafic enclave (table 2). The results show, after some AFC modeling by Kullberg (2015) that the relation between fractional crystallization and assimilation is 0.05, indicating little contamination.

7.4 HAOM

At the investigated location there is not yet any orthopyroxene megacrysts found. There is a possibility that there are HAOM, only that they have not been found yet. If there are in fact no HAOM this means that the required high pressure, accompanied by high aluminum concentration in the melt required was not reached. These factors are required for reaching the stability where orthopyroxene megacrysts can crystallize together with plagioclase megacrysts in a plagioclase saturated magma (Duchesne *et al*. 1999; Schiellerup *et al*. 2000; Charlier *et al*. 2010; Vander Auwera *et al*. 2011; Bybee *et al*. 2014; Chen *et al*. 2015).
Årebäck (1995) show that parent magma for the Hakefjorden Complex is high in Al, but since there is so much plagioclase the orthopyroxene is poor in Al, which could be the key factor in why there are no HAOMs found.

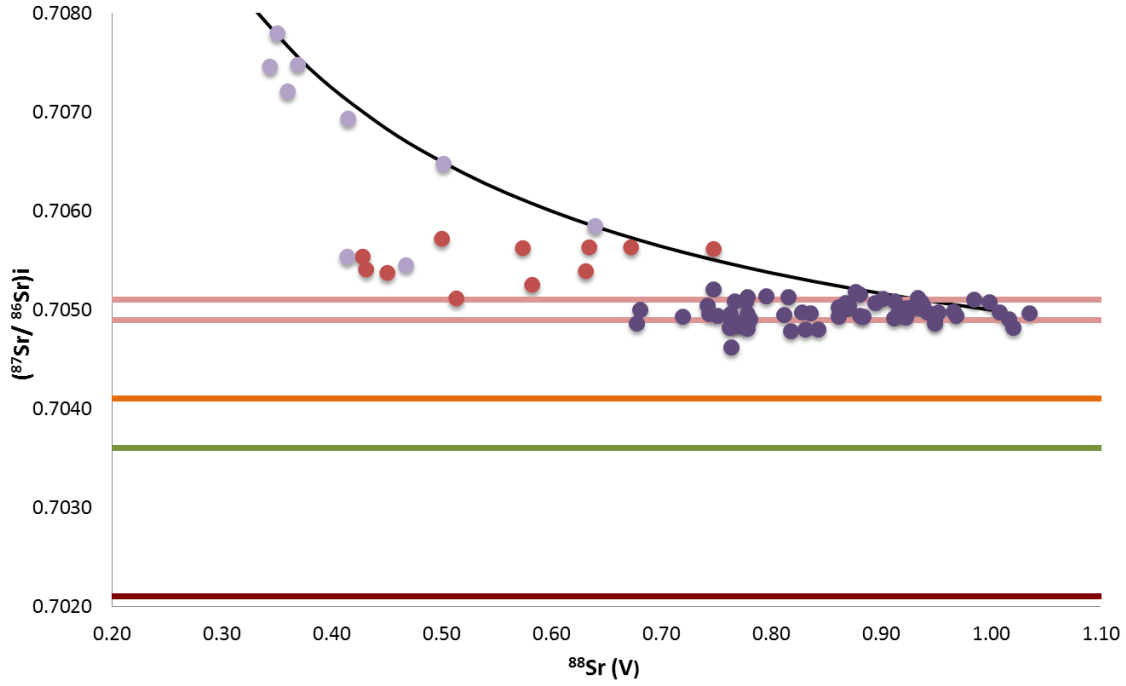

Fig. 21. Shows the Sr analytical results together with a mixing cure, showing contamination. The mixing goes up to the left in the diagram following the mafic enclave and mixing curve. The majority of the Hakefjorden rock units are in the dark purple, the hybrid matrix is red dots and the megacryst in the mafic enclave in light purple. They show little contamination in the vertical led, only horizontal variation show differentiation. The mafic enclave plots over all the other values, in two different areas, depending on where in the rock it is. The hybrid matrix plots between the Hakefjorden main rocks and the core of the megacryst in the enclave with significantly higher Sr signature. The red line is depleted mantle, the green is CHUR, the orange is Idefjorden mafic crust and the pink are the mean values.

7.5 Age of the Hakefjorden Complex

Hellström *et al*. (2004) have discovered that the Gothenburg dykes cut the contact aureole around the intrusion on Brattön. The Gothenburg dykes are 935 Ma indicating that the island is older than what current dating shows (Scherstén *et al*. 2000). Scherstén *et al*. (2000) dated the contact melt around the intrusion to 916 ±10 Ma. This means the only existing age is for crystallization of the contact melt and not for the emplacement or crystallization of the intrusion. After SEM investigations both zircon and baddeleyite have been identified, making it possible to date the intrusion directly.

7.6 Correlated magmatic events

The three anorthosite complexes, Egersund-Ogna, Håland-Hellered and Åna-Sira in the Rogaland province are all dated to have a connection to the magmatic event in the area around 930 Ma. The biggest magmatic plus between 933–929 Ma and then a smaller one between 920–916 Ma (Schärer *et al*. 1996; Duchesne 1999; Bolle *et al*. 2003; Charlier *et al*. 2010; Vander Auwera *et al*. 2011). The available dating for the intrusion (Scherstén *et al*. 2000) correlates to the magmatic pulses giving rise to the anorthosite complexes in Norway. So the time constrains are good, but if more correlation can be found between them is difficult to establish. If this was a larger magmatic event, underplating Rogaland it could have initiated the formation of the Hakefjorden Complex as well (Vander Auwera *et al*. 2011). Sr-isotope ratios from that area are similar to the ones found in the complex on Älgön, in the lower spectrum from 0,7040–0,7070 correlating to primitive jotunites in Rogaland (Vander Auwera *et al*. 2011). Another factor that bind them together is the results from Vander Auwera *et al*. (2011), which show that little contamination in the Rogaland anorthosite complexes has occurred.

7.7 Emplacement model of HFC

All samples have been altered, by late stage magmatic fluids after igneous crystallization. This is seen mostly in the altered norite, and the monzonorite.

The Sr-isotope ratios show an enriched signature if compared to both depleted mantle and CHUR (Fig. 21). The combined results from this study and Kullberg (2015) indicate that the intrusion is unmetamorphosed, and not much contamination has occurred. This means, that to explain the origin of Älgön only few sources fit. Firstly a lower crustal source, melt from mafic crust can be modeled to fit as source. This fits with the lower crust of the Idefjorden terrane, that could be the source for the parental melt (Fig. 21). Another plausible case is a mantle component enriched by subduction . But the latter is not possible looking at the results from Kullberg (2015). The main rock units on Älgön lack a double dip for Ta and Nb in trace element spiderdiagrams which is a good indication of a subduction related origin (Kullberg 2015). The high amounts of large-ion lithophile elements also contradict a subduction origin, since they are mobile when fluids affect the rock (Kullberg 2015). The rare earth elements and incompatible trace elements show an enrichment compared to an enriched mantle and CHUR (Kullberg 2015).

Oscillatory variation in the plagioclase could be an indication of the currents in the magma chamber, and that the plagioclase traveled up and down the chamber, changing the An-composition periodically due to change in pressure. But this is not because of pressure variation but because the An will not be stable for the entire crystallization sequence, but will gradually decrease. But as there is no clear zonation in the megacrysts in the main rock units, only in those found in the mafic enclave no good conclusions can be taken looking at the An variation in the megacrysts.

The theory of emplacement is presented in figure 22, similar to the original theory as suggested by Årebäck (1995). The theory for the IRL emplacement is connected to the theory presented here, and can be studied in further detail in Kullberg (2015) .

8 Conclusions

- The results from this study show that the plagioclase has higher An-content than shown by previous studies.
- The matrix in the IRL was the first to crystallize, based on the high An-content compared to the other rock units.
- The norite matrix, the anorthosite and the plagioclase megacrysts followed the IRL, all subsequently crystallizing after the IRL matrix.
- The variation seen in An and initial $^{87}Sr/^{86}Sr$ is most dependent of magma chemistry, not pressure that's responsible for the An and Sr variation in the rock units.
- The mafic enclaves has low An-values, which indicate late crystallization or contamination from other source. The Sr-ratios also indicate another evolution than the rest of the intrusion, with a Sr- isotopic signature suggesting crustal input.
- The Sr results and the An content show that the magma was homogenous when the rock units crystallized.
- Small variation in Sr-isotopic ratios amongst the main rock units, only the mafic enclaves and hybrid matrix deviates from this trend, indicating more crustal input.
- There has not been much contamination. The system has undergone differentiation.
- A lower mafic crustal source is interpreted to origin for the intrusion, based on the $^{87}Sr/^{86}Sr$.

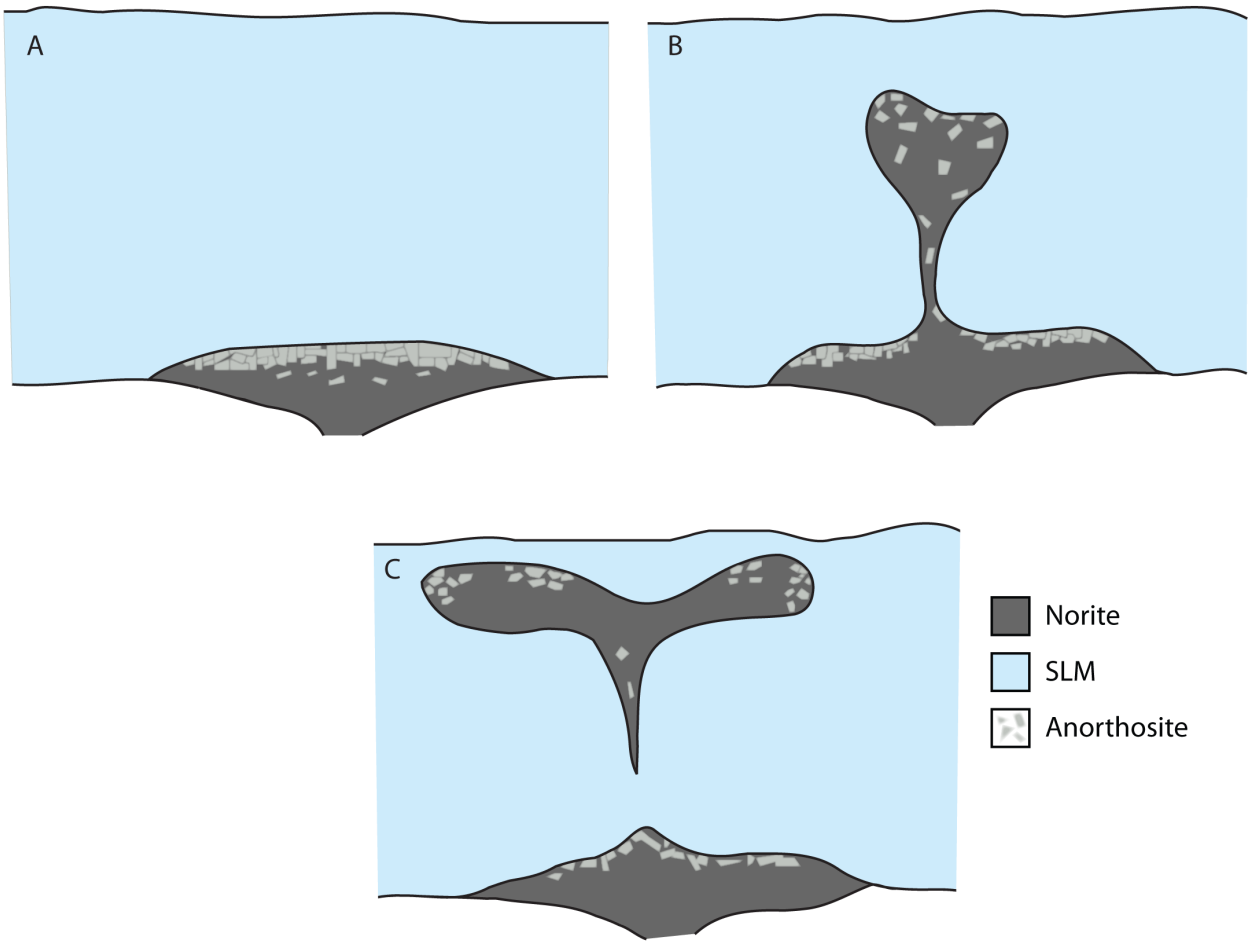

Fig. 22. Figure 21 A simplified emplacement theory for the island, based on the model proposed by Årebäck 1995, Årebäck & Stigh 1997, together with other similar theories. A) The first step of the islands evolution, with plagioclase starting to crystalize. The plagioclase will float to the top of the magma chamber, since it's got a lower density than the rest of the HFC rocks. The heavier IRL will accumulate on the bottom of the chamber. For the parallel IRL evolution and its emplacement see Kullberg 2015. B) The second stage of the evolution is an adiabatic rise due to the gravitational instability or more input of magma, dragging up the anorthosite fragments when rising. During this stage disequilibrium can be seen in the megacrysts in the inner patchy rim. The magma input have to be of the same source as the Sr-isotopes are homogenous through all the rock units except the mafic enclave and hybrid matrix. C) The last and final stage of the emplacement. The two island, Älgön (left) and Brattön (right) are set at upper crustal levels. Currents in the magma chamber are the reason the anorthosite blocks accumulate at the ends of the islands. The megacrysts continued to grow normally outside the inner rim. Due to currents and different density for the IRL compared to the rest of the rock units the IRL accumulate and is emplaced in the middle of the island. Since the IRL started to crystalize early it already had a lot of crystal mush when emplaced. This meant that the complex started to cool/crystallize from the inside out, and not the normal way from the edge to the center of the intrusion. For more detail on the magma currents, IRL emplacement see Kullberg 2015.

9 What comes next

After a closer look baddeleyite and zircon was identified in all samples, making direct dating possible. This could help to unravel the crystallization sequence and to improve the understanding of the islands evolution. Another step would be to do more Sr-isotope analysis on the rock units. Further investigations of the mafic enclave, as it was the only one of the rock units deviating from the main group. Take additional samples to get a more statistical correct representation of the island, or do more analysis on the samples already collected. A more detailed mapping of the island is needed to find the accurate relations between the different rock units.

10 Acknowledgements

First of all I would like to thank Sara Kullberg my close coworker during this entire study, for support, and encouragement. Second I would like to thank Andreas Petersson for all the help along the way. I would like to thank my supervisor Anders Scherstén. I would like to thank the research team at GTK, Geological survey of Finland for help with the MC-ICP-MS work. My family and friends for boosting my spirit during the times when it seemed too hard to continue. Lastly I would like to thank Martin and Eva Fahlén for lending their summerhouse as a research station during our time in the field.

11 References

Åhäll, K.I., Cornell, D.H. & Armstrong, R., 1998: Ion probe zircon dating of metasedimentary units across the Skagerrak: new constraints for early Mesoproterozoic growth of Baltic Shield. *Precambrian Research* 87, 117–134.

Åhäll, K.I. & Connelly, J.N., 2008: Long-term convergance along SW Fennoscandia: 330m.y. of Proterozoic crystal growth. *Precambrian Research* 163, 402–421.

Åhäll, K.I. & Daly J.S., 1989: Age, Tectonic Setting and Provenance of Östfold-Marstrand Belt Supracrustals:Westwards Crustal Growth of the Baltic Shield at 1760 Ma. *Precambrian research* 45, 45 –61.

Årebäck, H., 1995: *The Hakefjorden complex, geology and petrogenesis of a late Sveconorwegian norite -anorthosite intrusion, south-west Sweden*. Earth sciences center Göteborg University A9Department of Geology Göteborg. 84Pp .

Årebäck, H. & Andersson, U.B., 2002: Granulite-facies contact metamorphism around the Hakefjorden Norite-Anorthosite Complex, SW Sweden. *Norwegian journal of geology* 82, 29–44.

Årebäck, H., Andersson, U.B. & Petersson J., 2008: Petrological evidence for crustal melting, unmixing, and undercooling in an alkali-calcic, high-level intrusion: the late Sveconorwegian Vinga intrusion, SW Sweden. *Mineralogy and Petrology* 93, 1–46.

Årebäck, H. & Stigh, J., 1997: Polybaric evolution of the Hakefjorden Complex, southwestern Sweden, deduced from partial dissolution in andesine megacrysts. *GFF* 119, 97–101.

Årebäck, H., & Stigh, J., 2000: The nature and origin of an anorthosite associated ilmenite-rich leuconorite, Hakefjorden Complex, south-west Sweden. *Lithos* 51, 247–267.

Bergström, L., 1963: Petrology of the Tjörn area in western Sweden : an investigation of Archean sediments, their transformations and other petrological features 134 pp.

Bingen, B., Nordgulen, Ø. & Viola, G., 2008: A four-phase model for the Sveconorwegian orogeny, SW Scandinavia. *Norwegian Journal Of Geology* 88, 43–72.

Blundy, J.D. & Wood, B.J., 1991: Crystal-chemical controls on the partitioning of Sr and Ba between plagioclase feldspar, silicate melts, and hydrothermal solutions. *Geochemica et Cosmochimica Acta* 55, 193–209.

Bolle, O., Demaiffe, D. & Duchesne, J.C. 2003: Petrogenesis of jotunitic and acidic members of an AMC suite (Rogaland anorthosite province, SW Norway) a SR and Nd isotopic assessment. *Precambrian Research* 124, 185–214.

Bowen, N. L., 1922: The Reaction Principle in Petrogenesis. *The Journal of Geology* vol. 30 no. 3, 177–198.

Brewer, T.S., Daly, J.S. & Åhäll, K.I., 1998: Contrasting magmatic arcs in the Paleoproterozoic of the south-western Baltic Shield. *Precambrian Research* 92, 297–315.

Bybee, G.M., Ashwal, L.D., Shirey, S.B., Horan, M., Mock, T. & Andersen, T.B., 2014: Pyroxene megacrysts in Proterozoic anorthosites: Implications for tectonic settin, magma source and magmatic processes at the Moho. *Earth and Planetary Science Letters* 389, 74–85.

Charlier, B., Duchesnes, J.C., Vander Auwera, J., Strome, J.Y., Maquil, R. & Longhai, J., 2010: Polybaric Fractional Crystallization of High-alumina Basalt Parental Magmas in the Egersund -Ogna Massif-type Anorthosite (Rogaland, SW Norway) Constrained by Plagioclase and High-alumina Orthopyroxene Megacrysts. *Journal of Petrology* 51 (12), 2515–2546.

Chen, W.T., Zhou, M.F., Gao, J.F. & Zhao, T.P., 2015: Oscillatory Sr isotopic signature in plagioclase megacrysts from the Damiao anorthosite complex, Norther China: Implication for petrogenesis of massif-type anorthosite. *Chemical Geology* 393–394, 1–15.

Daly, J.S., Park, R.G. & Cliff, R.A., 1979: Rb-Sr of intrusive plutonic rocks from Stora Le-Marstand belt in orust, SW Sweden. *Precambrian Research* 9, 189–198.

Duchesnes, J, 1999: Fe-Ti in Rogaland anorthosites (South Norway) geochemical characteristics and problems of interpretation. *Mineral DepositaI* 34, 182–198.

Duchesnes, J, C., Liégeois, J, P., Vander Auwera, J. & Longhai, J., 1999: The crustal tounge melting model and the origin of massive anorthosites. *Terra Nova* 11, 100–105.

Ebbing, J., Afework, Y., Oelsen, O. & Nordgulen, Ø. 2005: Is there evidence for magmatic underplating beneath the Oslo rift? *Terra Nova* 17, 129–134.

Eliasson, T., Ahlin, S. & Petersson, A., 2003: Emplacement mechanism and thermobarometry of the Sveconorwegian Bohus granite, SW Sweden. *GFF* 125, 113–130.

Eliasson, T. & Schröberg, H., 1991: U-Pb dating of the post kinematic Sveconorwegian (Grenvillian) Bohus granite, SW Sweden: evidence of restitic zircon. *Precambrian Research* 51, 337–350.

Fahlén, M., Stigh, J., & Årebäck, H., 2008: *Strövtåg på Bohusläns sockertopp*. AMFO-klinikdata 96 pp.

Gorbatschev, R. & Bogdanova, S., 1993: Frontiers in the Baltic Shield. *Precambrian Research* 64, 3–21.

Hellström, F.A., Johansson, Å. & Larson, S.Å., 2004: Age and emplacement of late Sveconorwegian monzogabbroic dykes, SW Sweden. *Precambrian Research* 128, 39–55.

Johansson, Å., Meier, M., Oberli, F., & Wikman, H., 1993: The early evolution of the Southwest Swedish Gneiss Province: geochronological and iso-

topic evidence from southernmost Sweden

Kullberg, S., 2015: Using Fe-Ti and trace element analysis to determine crystallization sequence of an anorthosite-norite intrusion Älgön, SW Sweden. *Dissertations in Geology at Lund University,* No 454, 32 pp.

Lindsley, D:H., 1971: Melting relations of plagioclase at high pressure. *NEW YORK state museum and science service memoir* 18, 39–46.

Ljunger, E., 1927: Spaltentektonik und Morphologie der Schwedishen Skagerrak-Kuste. *Bulletin of the Geological Institution of the University of Uppsala* 21, 26–29.

Longhi, J., Fram, M.S., Vander Auwera, J. & Montieth, N.J., 1993: Pressure effects, kinetics, and rheology of anorthositic and related magmas. *American Mineralogy* 78, 1016–1030.

Longhai, J., Vander Auwera, J., Fram, M.S. & Duchesne, J.C., 1999: Some phase equilibrium constraints on the origin of Proterozoic (massif) anorthosite and related rocks. *Journal of Petrology* 40, 339–362.

Lundquist, T., 1979: The Precambrian of Sweden. Geology of the European countries SGU 789, 87pp.

Markl, G. & Höhndorf, A., 2003: Isotopic constraints on the origin of AMCG-suite rocks on the Lofoten Islands, N Norway. *Mineralogy and Petrology* 78, 149–171.

Müller, W., M. Shelley, Miller, P. & Broude, S., 2009: Initial performance metrics of a new custom-designed ArF excimer LA-ICPMS system coupled to a two-volume laser-ablation cell. *Journal of Analytical Atomic Spectrometry* 24, 209–214.

Möller, C., Andersson, J., Lundqvist, I. & Hellström, F., 2007: Linking deformation, migmatite formation and zircon U-Pb geochronology in polymetamorphic orthogneisses, Sveconorwegian Province, Sweden. *Journal of Metamorphic Geology* 25, 727–750.

Nebel, O., Scherer, E.E. & Mezger, K., 2011: Evaluation of the 87Rb decay constant by age comparison against the U–Pb system. *Earth and Planetary Science Letters* 301, 1–8.

Panjasawatwong, Y., Danyushevsky, L.V., Crawford, A.J. & Harris, K.L., 1995: An experimental study of the effects of melt composition on plagioclase – melt equilibria at 5 and 10 kbar: implications for the origin of magmatic high-An plagioclase. *Contribution Mineral Petrology* 118, 420–432.

Park, R.G., Åhäll, K.I. & Boland., M.P., 1991: The Sveconorwegian shear-zone network of SW Sweden in relation to mid-Proterozoic plate movements. *Precambrian Research* 49, 245–260.

Petersson, A., Scherstén, A., Bingen, B., Gerdes, A. & Whitehouse, M.J., 2015: Mesoproterozoic continental growth: U-Pb-Hf-O zircon record in the Idefjorden Terrane, Sveconorwegian Orogen. *Precambrian Research* 261, 75–95

Rankenburg, K., Lassiter, J.C. & Brey, G., 2004: Origin of megacrysts in volcanic rocks of the Cameroon volcanic chain - constraints on magma genesis and crustal contamination. *Contribution to Mineralogy and Petrology* 147, 129–144.

Scherstén, A., Årebäck, H., Cronell, D., Hoskin, P., Åberg, A. & Armstrong, R., 2000: Dating mafic-ultramafic intrusions by ion-microprobing contact -melt zircon: examples from SW Sweden. *Contribution Mineral Petrology* 139, 115–125.

Schiellerup. H., Lambert, D.D., Persvik, T., Robins, B., McBride, J.S. & Larsen, R.B, 2000: Re-Os isotopic evidence for a lower crustal origin of massif-type anorthosites. *Nature 405, 781–784*.

Schärer, U., Wilmart, E. & Duchesne, J.C., 1996: The short duration and orogenic character of anorthosite magmatism: U-Pb dating of the Rogaland complex Norway. *Earth and Planetary Science Letters* 139, 335–350.

Slagstad, T., Roberts, N.M., Marker, M., Røhr, T.S. & Schiellerup. H., 2013: A non-collisional, accretionary Sveconorwegian orogen. *Terra Nova* 25, 30–37.

Söderlund, U., Jarl, L.G., Persson, P.O., Stephens., M.B. & Whalgern, C.H., 1999: Protolith ages and timing of deformation in the eastern, marginal part of the Sveconorwegianm orogeny, southwestern Sweden. *Precambrian Research* 94, 29–48.

Söderlund, U., Isachsen, C.E., Bylund, G., Heaman, L.M., Patchett, P.J., Vervoort, L.M. & Andersson, U.B., 2005: U-Pb baddeleyite ages and Hf, Nd misotope chemistry constraining repeated mafic magmatism in the Fennoscandian Shield from 1.6 to 0.9 Ga. *Contributions to Mineralogy and Petrology* 150, 174–194.

Ustunisik, G., Kilinc, A. & Nielsen, R.L., 2014: New insights into the processes controlling compositional zoning in plagioclase. *Lithos* 200–201, 80–93.

Vander Auwera, J., Bolle, O., Bingen, B., Liégeois, J.P., Bogaerts, M. & Duchesnes, J.C., 2011: Sveconorwegian massif type anorthosites and related granitoids result from post-collisional melting of a continental arc root. *Earth-Sciense Reviews* 107, 375–397.

Vander Auwera, J., Longhai, J. & Duchesne, J.C., 2000: The effect of pressure on D_{Sr} (plag/melt) and D_{Cr} (opx/melt): implications for anorthosite petrogenesis. *Earth and Planetary Science Letters* 178, 303–314.

Winter, J.D. 2010: *Principals of Igneous and Metamorphic Petrology second edition*. Pearson,Prentice Hall 702pp.

Wiszniewska, J., Cleasson, S., Stein, H., Vander Auwera, J. & Duchesne, J.C., 2002: The northeastern Polish anorthosite massifs: petrological, geochemical and isotopic evidence for a crustal derivation. *Terra Nova* 14, 451–460.

Sample nr	Rock description	North-Latitude	East-Longitude
AGSE03	Norite with plagioclase megacryst	57°55.365	011°40.787
AGSE04	Norite with plagioclase megacryst	57°55.365	011°40.787
AGSE05	Quartz vein in norite	57°55.365	011°40.787
AGSE06	Plagioclase megacryst	57°55.365	011°40.787
AGSE07	Anorthosite	57°55.502	011°40.916
AGSKSE03(1)	IRL-matrix	57°55.434	011°41.095
AGSKSE03(2)	IRL-matrix	57°55.434	011°41.095
AGSKSE03(3)	IRL-matrix	57°55.434	011°41.095
AGSKSE04	Altered norite	57°55.491	011°41.119
AGSKSE06	IRL-altered norite	57°55.431	011°41.121
AGSKSE08	IRL-matrix	57°55.431	011°41.121
AGSKSE09(1)	Altered norite	57°55.430	011°41.107
AGSKSE09(2)	Altered norite	57°55.430	011°41.107
AGSKSE10	Norite	57°55.431	011°41.121
AGSKSE11	Magnetic vein	57°55.431	011°41.121
AGSKSE17	Oxide aggregate	57°55.455	011°41.125
AGSKSE18	Altered gabbro	From profile 1	
AGSKSE21(1)	Mafic enclave	57°55.369	011°40.703
AGSKSE21(2)	Mafic enclave	57°55.369	011°40.703
AGSKSE22(1)	Altered norite	57°55.369	011°40.736
AGSKSE22(2)	Altered norite	57°55.369	011°40.736
AGSKSE23	Altered norite	57°55.460	011°41.187
AGSKSE24	SLM	57°55.233	011°41.880
AGSKSE25	Monzonorit	57°55.363	011°41.388

Rock	Plagioclase type	^{88}Sr (V)	$^{87}Rb/^{86}Sr$	$^{87}Sr/^{86}Sr$	1s	Rb/Sr	$(^{87}Sr/^{86}Sr)_i$	2s	Age Ga
Norite with plagioclase megacryst									
1	Megacryst	0.87	0.0063	0.70510	0.00002	0.00230	0.70502	0.00004	0.900
2	Megacryst	0.86	0.0101	0.70513	0.00002	0.00363	0.70500	0.00005	0.900
3	Megacryst	0.88	0.0119	0.70530	0.00002	0.00436	0.70515	0.00005	0.900
3.2	Megacryst	0.68	0.0096	0.70498	0.00003	0.00353	0.70486	0.00006	0.900
4	Megacryst	0.88	0.0140	0.70511	0.00002	0.00507	0.70494	0.00005	0.900
5	Megacryst	0.88	0.0156	0.70538	0.00002	0.00520	0.70518	0.00005	0.900
6	Megacryst	0.82	0.0050	0.70519	0.00002	0.00183	0.70513	0.00005	0.900
7	Matrix	0.83	0.0072	0.70507	0.00002	0.00250	0.70497	0.00005	0.900
8	Megacryst	0.78	0.0127	0.70507	0.00003	0.00459	0.70491	0.00006	0.900
9	Megacryst	0.72	0.0082	0.70503	0.00003	0.00303	0.70493	0.00005	0.900
10	Megacryst	0.76	0.0048	0.70493	0.00003	0.00173	0.70487	0.00005	0.900
11	Megacryst	0.75	0.0047	0.70500	0.00002	0.00169	0.70494	0.00005	0.900
12	Megacryst	0.76	0.0041	0.70487	0.00002	0.00154	0.70481	0.00005	0.900
13	Megacryst	0.76	0.0081	0.70472	0.00002	0.00294	0.70462	0.00005	0.900
14	Megacryst	0.77	0.0083	0.70519	0.00002	0.00309	0.70509	0.00005	0.900
15	Megacryst	0.80	0.0047	0.70519	0.00003	0.00177	0.70514	0.00005	0.900
16	Matrix	0.77	0.0077	0.70494	0.00003	0.00284	0.70484	0.00005	0.900
Anorthosite									
1	Anorthosite	0.68	0.0070	0.70509	0.00003	0.00258	0.70500	0.00006	0.900
2	Anorthosite	0.82	0.0097	0.70491	0.00002	0.00359	0.70479	0.00005	0.900
3	Anorthosite	0.83	0.0077	0.70490	0.00002	0.00283	0.70480	0.00005	0.900
4	Anorthosite	0.81	0.0066	0.70503	0.00002	0.00244	0.70495	0.00005	0.900
5	Anorthosite	0.77	0.0065	0.70492	0.00002	0.00241	0.70484	0.00005	0.900
6	Anorthosite	0.76	0.0063	0.70503	0.00003	0.00232	0.70495	0.00005	0.900
IRL-matrix									
1	Anorthosite	0.87	0.0165	0.70528	0.00002	0.00571	0.70507	0.00006	0.900
2	Anorthosite	0.90	0.0061	0.70519	0.00002	0.00215	0.70511	0.00005	0.900
3	Anorthosite	0.95	0.0036	0.70502	0.00002	0.00132	0.70498	0.00004	0.900

4	Anorthosite	0.87	0.0064	0.70512	0.00002	0.00213	0.70504	0.00005	0.900
5	Anorthosite	0.89	0.0141	0.70525	0.00002	0.00491	0.70507	0.00006	0.900
7	Matrix	0.95	0.0064	0.70494	0.00002	0.00240	0.70486	0.00004	0.900
8	Matrix	0.95	0.0061	0.70497	0.00002	0.00226	0.70489	0.00004	0.900
9	Matrix	0.94	0.0049	0.70510	0.00002	0.00181	0.70504	0.00004	0.900
10	Matrix	0.91	0.0113	0.70523	0.00002	0.00349	0.70508	0.00006	0.900
11	Snowflake	0.92	0.0075	0.70508	0.00002	0.00276	0.70499	0.00005	0.900
12	Matrix	0.92	0.0069	0.70508	0.00002	0.00255	0.70500	0.00004	0.900
13	Matrix	0.92	0.0065	0.70501	0.00002	0.00222	0.70493	0.00005	0.900
IRL-matrix									
1	Snowflake	0.93	0.0060	0.70520	0.00002	0.00220	0.70512	0.00005	0.900
2	Snowflake	0.94	0.0077	0.70518	0.00002	0.00281	0.70508	0.00004	0.900
3	Snowflake	0.92	0.0079	0.70511	0.00002	0.00295	0.70501	0.00005	0.900
4	Snowflake	0.87	0.0202	0.70527	0.00002	0.00700	0.70501	0.00006	0.900
IRL-matrix									
1	Matrix	1.04	0.0094	0.70509	0.00002	0.00348	0.70497	0.00004	0.900
2	Matrix	1.01	0.0176	0.70519	0.00002	0.00594	0.70497	0.00006	0.900
4	Grey inclusion	0.99	0.0155	0.70530	0.00004	0.00406	0.70510	0.00009	0.900
5	Grey inclusion	1.00	0.0056	0.70515	0.00002	0.00194	0.70508	0.00005	0.900
6	Snowflake	1.02	0.0048	0.70497	0.00002	0.00176	0.70491	0.00004	0.900
7	Snowflake	1.02	0.0188	0.70505	0.00002	0.00674	0.70482	0.00005	0.900
8	Snowflake	0.97	0.0087	0.70505	0.00002	0.00310	0.70494	0.00005	0.900
9	Snowflake	0.97	0.0090	0.70509	0.00002	0.00323	0.70498	0.00004	0.900
Magnetic vein									
1	Matrix	0.95	0.0038	0.70501	0.00002	0.00138	0.70496	0.00005	0.900
2	Matrix	0.94	0.0107	0.70511	0.00002	0.00398	0.70497	0.00005	0.900
3	Matrix	0.92	0.0053	0.70508	0.00002	0.00190	0.70502	0.00005	0.900
4	Matrix	0.92	0.0065	0.70505	0.00002	0.00239	0.70496	0.00005	0.900
5	Matrix	0.93	0.0126	0.70519	0.00002	0.00459	0.70503	0.00005	0.900
6	Matrix	0.93	0.0071	0.70511	0.00002	0.00263	0.70502	0.00005	0.900

Oxide concentration									
1	Snowflake	0.91	0.0053	0.70498	0.00002	0.00193	0.70491	0.00005	0.900
2	Snowflake	0.78	0.0084	0.70524	0.00002	0.00314	0.70513	0.00005	0.900
3	Snowflake	0.84	0.0076	0.70482	0.00003	0.00274	0.70472	0.00005	0.900
4	Anorthosite	0.78	0.0093	0.70493	0.00002	0.00343	0.70481	0.00004	0.900
5	Anorthosite	0.75	0.0085	0.70531	0.00002	0.00310	0.70521	0.00004	0.900
6	Anorthosite	0.78	0.0074	0.70518	0.00003	0.00274	0.70509	0.00005	0.900
7	Anorthosite	0.84	0.0087	0.70491	0.00003	0.00313	0.70480	0.00006	0.900
8	Anorthosite	0.88	0.0095	0.70505	0.00002	0.00342	0.70493	0.00005	0.900
9	Anorthosite	0.84	0.0031	0.70501	0.00002	0.00112	0.70497	0.00005	0.900
10	Snowflake	0.74	0.0061	0.70504	0.00003	0.00225	0.70496	0.00005	0.900
11	Snowflake	0.78	0.0080	0.70499	0.00002	0.00291	0.70489	0.00005	0.900
Mafic enclave with hybrid matrix									
1	Megacryst	0.35	0.0195	0.70804	0.00006	0.00721	0.70779	0.00012	0.900
2	Megacryst	0.36	0.0261	0.70754	0.00004	0.00938	0.70721	0.00010	0.900
3	Megacryst	0.34	0.0251	0.70777	0.00005	0.00926	0.70745	0.00010	0.900
4	Megacryst	0.47	0.0488	0.70607	0.00004	0.01742	0.70545	0.00010	0.900
5	Matrix	0.50	0.0210	0.70598	0.00004	0.00728	0.70572	0.00008	0.900
6	Matrix	0.57	0.0099	0.70575	0.00003	0.00359	0.70562	0.00007	0.900
7	Matrix	0.63	0.0105	0.70577	0.00003	0.00386	0.70563	0.00007	0.900
8	Matrix	0.43	0.0369	0.70600	0.00004	0.01317	0.70553	0.00010	0.900
10	Matrix	0.67	0.0394	0.70613	0.00003	0.01415	0.70563	0.00007	0.900
11	Matrix	0.43	0.0486	0.70602	0.00004	0.01759	0.70541	0.00011	0.900
12	Matrix	0.45	0.0485	0.70598	0.00004	0.01855	0.70537	0.00011	0.900
13	Megacryst	0.50	0.0156	0.70667	0.00003	0.00573	0.70647	0.00007	0.900
14	Megacryst	0.37	0.0389	0.70797	0.00004	0.01390	0.70748	0.00011	0.900
15	Megacryst	0.42	0.0187	0.70716	0.00005	0.00696	0.70693	0.00010	0.900
16	Megacryst	0.64	0.0113	0.70599	0.00003	0.00410	0.70584	0.00006	0.900
19	Matrix	0.63	0.0373	0.70586	0.00003	0.01172	0.70538	0.00009	0.900
20	Matrix	0.58	0.0266	0.70558	0.00003	0.00911	0.70525	0.00008	0.900

21	Matrix	0.51	0.0361	0.70557	0.00003	0.01330	0.70511	0.00008	0.900
22	Matrix	0.75	0.0063	0.70569	0.00002	0.00232	0.70561	0.00005	0.900
23	Matrix	0.41	0.1149	0.70699	0.00005	0.04218	0.70553	0.00014	0.900
Altered norite									
1	Megacryst	0.76	0.0075	0.70513	0.00002	0.00266	0.70503	0.00005	0.900
2	Megacryst	0.78	0.0044	0.70501	0.00003	0.00164	0.70495	0.00006	0.900
3	Megacryst	0.74	0.0065	0.70512	0.00002	0.00233	0.70504	0.00005	0.900
4	Matrix	0.86	0.0041	0.70508	0.00002	0.00150	0.70503	0.00004	0.900
5	Megacryst	0.86	0.0054	0.70500	0.00003	0.00199	0.70493	0.00005	0.900

Sample AGSE03													
Plagioclase	Megacryst							Matrix					
Analytical point	1							2					
Spectrum	1	2	3	4	5	6	7	1	2	3	4	5	6
Na	4.93	4.96	5.11	5.07	4.23	4.35	5.21	4.39	4.98	5.11	4.61	5.19	4.44
Al	14.14	14.62	14.64	14.83	16.53	16.85	16.44	15.33	14.24	14	13.94	12.41	13.49
Si	27.58	28.06	28.59	29	27.82	28.25	29.82	25.89	26.89	26.57	25.51	23.42	24.06
K	0.68	0.49	0.68	0.74	0.49	0.38	0.42	0.3	0.6	0.75	0.58	0.46	0.38
Ca	6.35	6.48	6.39	6.7	8.65	8.76	7.71	7.74	6.31	5.89	6.32	6.85	6.44
O	48.54	49.51	50.13	50.89	51.54	52.34	53.65	47.9	47.82	47.1	45.81	42.65	43.74
Fe	0.52	0.42	0.28	0.25	0.39	0.27	0.3	0.31	0.49	0.34	0.36	1.05	0.44
Totals	102.76	104.54	105.81	107.47	109.66	111.21	113.55	101.85	101.33	99.77	97.13	92.02	93.01
An	53.09	54.32	52.46	53.56	64.70	64.94	57.80	62.27	53.07	50.13	54.91	54.80	57.19
Ab	41.22	41.58	41.95	40.53	31.64	32.25	39.06	35.32	41.88	43.49	40.05	41.52	39.43
Or	5.69	4.11	5.58	5.92	3.66	2.82	3.15	2.41	5.05	6.38	5.04	3.68	3.37

Sample AGSE03														
Plagioclase	Megacryst							Matrix						
Analytical point	3							10						
Spectrum	1	2	3	4	5	6	7	1	2	3	4	5	6	7
Na	4.63	4.9	5.04	5.23	5.27	4.64	3.79	4.71	4.5	4.58	4.7	4.93	4.47	4.56
Al	13.48	14.48	14.96	15.26	14.43	13.81	11.69	16.23	16.32	16.19	16.27	15.89	15.71	15.46
Si	26.11	27.59	28.89	29.3	29.06	26.13	21.66	27.73	27.99	27.99	28.17	28.45	27.53	27.43
K	0.5	0.5	0.57	0.62	0.69	0.44	0.41	0.15	0.29	0.32	0.29	0.28	0.81	0.38
Ca	6.2	6.58	6.82	6.93	6.29	6.38	5.49	8.31	8.23	8.43	8.06	7.72	7.8	7.63
O	46.02	48.84	50.91	51.71	50.58	46.41	38.76	51.05	51.3	51.33	51.45	51.38	50.19	49.85
Fe	0.32	0.34	0.33	0.17	0.55	0.39	0.3	0.03		0.02			0.01	0.2
Totals	97.27	103.24	107.51	109.22	106.85	98.2	82.09	108.21	108.63	108.86	108.94	108.65	106.52	105.51
An	54.72	54.92	54.87	54.23	51.35	55.67	56.66	63.10	63.21	63.24	61.76	59.71	59.63	60.70
Ab	40.86	40.90	40.55	40.92	43.02	40.49	39.11	35.76	34.56	34.36	36.02	38.13	34.17	36.28
Or	4.41	4.17	4.59	4.85	5.63	3.84	4.23	1.14	2.23	2.40	2.22	2.17	6.19	3.02

Sample AGSE03														
Plagioclase	Megacryst													
Analytical point	11													
Spectrum	1	2	3	4	5	6	7	8	9	10	11	12	13	14
Na	4.11	3.91	4.03	4.36	4.47	4.62	4.83	4.78	4.78	4.92	6.39	4.98	4.65	4.4
Al	12.29	13.67	14.28	14.27	14.66	14.98	15.27	15.55	15.62	15.71	14.38	14.8	13.64	13.47
Si	22.96	23.72	24.67	26.1	26.57	27.4	28.09	28.1	28.48	28.59	30.02	27.48	27.26	25.45
K	0.35	0.2	0.49	0.48	0.55	0.51	0.55	0.61	0.46	0.52	0.39	0.44	1.48	0.59
Ca	5.82	7.01	7.3	7.11	7.21	7.12	7.31	7.51	7.62	7.47	5.64	6.87	5.97	6.22
O	40.91	43.37	45.22	46.87	47.86	49.1	50.29	50.63	51.14	51.35	51.54	49.03	47.49	45.11
Totals	86.44	91.88	95.99	99.19	101.32	103.73	106.34	107.18	108.1	108.56	108.36	103.6	100.49	95.24
An	56.61	63.04	61.76	59.50	58.95	58.12	57.60	58.22	59.25	57.86	45.41	55.90	49.34	55.49
Ab	39.98	35.16	34.09	36.49	36.55	37.71	38.06	37.05	37.17	38.11	51.45	40.52	38.43	39.25
Or	3.40	1.80	4.15	4.02	4.50	4.16	4.33	4.73	3.58	4.03	3.14	3.58	12.23	5.26

Sample AGSE03							Sample AGSE04							
Plagioclase	Megacryst						Plagioclas	Megacryst						
Analytical point		11.2					Analytical	1						
Spectrum	15	1	2	3	4	5	Spectrum	1	2	3	4	5	6	7
Na	4.18	4.97	4.74	4.62	4.23	4.76	Na	5.53	5.34	5.11	4.97	4.95	3.89	4.85
Al	12.33	14.56	14.93	15.07	15.51	15	Al	16.8	15.83	15.77	15.4	15.18	16.07	14.9
Si	23.7	28.19	27.5	27.61	26.93	27.72	Si	29.97	28.37	28.02	27.49	27.1	25.2	26.28
K	0.43	0.57	0.59	0.53	0.41	0.39	K	0.48	0.48	0.44	0.45	0.47	0.24	0.34
Ca	5.98	6.7	7.02	7.21	8.33	7.22	Ca	7.71	7.02	7.14	7	7.14	8.63	6.85
O	41.89	49.59	49.18	49.45	49.37	49.54	O	54.19	51.16	50.67	49.62	49.05	47.85	47.69
Totals	88.51	104.58	103.96	104.49	104.78	104.63	Totals	114.68	108.2	107.14	104.93	103.89	101.87	100.92
An	56.47	54.74	56.84	58.33	64.23	58.37	An	56.20	54.67	56.26	56.36	56.85	67.63	56.89
Ab	39.47	40.60	38.38	37.38	32.61	38.48	Ab	40.31	41.59	40.27	40.02	39.41	30.49	40.28
Or	4.06	4.66	4.78	4.29	3.16	3.15	Or	3.50	3.74	3.47	3.62	3.74	1.88	2.82

Sample AGSE04						AGSKSE03-1								
Plagioclase	Megacryst					Plagioclase	Inclusions						Matrix	
Analytical point	1.2					Analytical pc	1						3	5
Spectrum	1	2	3	4	5	Spectrum	1	2	3	4	5	6	1	1
Na	5.03	4.83	3.99	3.88	4.58	Na	3.79	3.61	3.97	3.16	3.5	3.35	4.46	3.86
Al	15.36	15.07	13.75	15.71	14.12	Al	15.48	15.57	15.19	16.2	15.57	15.71	14.99	15.47
Si	27.32	27.05	23.35	24.83	25.06	Si	25.93	25.98	26.55	25.21	25.74	25.8	27.36	26.36
K	0.44	0.48		0.3	0.83	K	0.41	0.43	0.47	0.39	0.53	0.78	0.49	0.5
Ca	7.27	7.05	10.34	8.68	6.5	Ca	8.61	8.56	7.86	9.58	8.67	8.59	7.22	8.07
O	49.64	48.9	44.67	47.22	45.57	O	48.15	48.21	48.38	48.13	47.96	48.13	49.03	48.45
Fe	0.4	0.29	1.14	0.29	0.36	Totals	102.37	102.38	102.42	102.67	101.97	102.37	103.55	102.71
Totals	105.45	103.67	97.24	100.9	97.02									
An	57.06	57.04	72.16	67.50	54.58	An	67.21	67.94	63.90	72.96	68.27	67.53	59.33	64.92
Ab	39.48	39.08	27.84	30.17	38.46	Ab	29.59	28.65	32.28	24.07	27.56	26.34	36.65	31.05
Or	3.45	3.88	0.00	2.33	6.97	Or	3.20	3.41	3.82	2.97	4.17	6.13	4.03	4.02

AGSKSE03-1													
Plagioclase	Matrix						Anorthosite						
Analytical point	7					9	11			13	15		
Spectrum	1	2	3	4	5	1	1	2	3	1	1	2	3
Na	4.01	4.07	4.01	4.04	4.07	3.97	3.93	4.16	3.78	4.03	3.83	3.72	3.72
Al	15.18	14.86	15.03	14.88	14.82	14.78	14.65	14.6	15.11	14.49	14.65	15.1	15.12
Si	25.92	25.98	25.87	25.66	25.92	25.45	26.26	26.51	25.35	25.72	26.08	25.64	25.72
K	0.64	0.66	0.51	0.48	0.58	0.51	0.57	0.6	0.36	0.55	0.46	0.37	0.42
Ca	7.66	7.54	7.65	7.72	7.35	7.53	7.68	7.11	8.35	7.32	7.73	8.36	7.92
O	47.62	47.38	47.4	47.05	47.17	46.82	47.51	47.59	47.04	46.62	47.26	47.35	47.29
Fe						0.68							
Totals	101.03	100.49	100.47	99.83	99.91	99.72	100.6	100.57	99.99	98.73	100.01	100.54	100.19
An	62.23	61.45	62.86	63.07	61.25	62.70	63.05	59.90	66.85	61.51	64.31	67.15	65.67
Ab	32.58	33.17	32.95	33.01	33.92	33.06	32.27	35.05	30.26	33.87	31.86	29.88	30.85
Or	5.20	5.38	4.19	3.92	4.83	4.25	4.68	5.05	2.88	4.62	3.83	2.97	3.48

AGSKSE03-2										Sample AGSKSE04			
Plagioclase	Matrix									Plagioclase	Matrix		
Analytical point	1			3						Analytical point	6		
Spectrum	1	2	4	2	3	4	5	6	7	Spectrum	1	2	3
Na	4.07	4.15	4.12	3.77	1.59	3.66	3.78	3.78	3.92	Na	4.22	4.04	4.09
Al	15.56	15.47	15.53	13.76	8.16	14.11	14.16	14.05	13.56	Al	16.51	15.86	15.26
Si	26.15	26.16	26.16	23.99	26.88	23.94	23.76	23.6	24.43	Si	26.15	25.6	24.92
Ca	8.09	8.06	7.86	0.63	0.39	0.52	0.51	0.53	0.74	K	0.37	0.36	0.26
O	48.28	48.35	48.3	6.96	3.23	7.31	7.25	7.17	6.16	Ca	8.48	8.3	8.06
K		0.6	0.51	43.79	41.96	44.12	43.98	43.67	43.87	Fe	0.48	0.56	0.29
Mg					2.3					O	49.54	48.23	46.74
Fe					2.25					Totals	105.74	102.95	99.62
Totals	102.15	102.78	102.49	92.89	86.75	93.66	93.66	92.81	92.67				
An	66.53	62.92	62.93	61.27	62.00	63.62	62.82	62.46	56.93	An	64.88	65.35	64.95
Ab	33.47	32.40	32.99	33.19	30.52	31.85	32.76	32.93	36.23	Ab	32.29	31.81	32.96
Or	0.00	4.68	4.08	5.55	7.49	4.53	4.42	4.62	6.84	Or	2.83	2.83	2.10

Sample AGSKSE04											Sample AGSE07		
Plagioclase	Matrix					Matrix					Plagioclas	Anorthosite	
Analytical point			7				8				Analytical	6	
Spectrum	4	5	1	2	3	4	1	2	3	4	Spectrum	1	2
Na	4.11	3.31	3.58	3.84	3.82	6.77	3.89	5.4	5.4	3.51	Na	4.54	4.33
Al	15.26	11.55	15.25	15.13	15.69	14.23	15.2	13.78	13.78	0.49	Al	14.53	14.28
Si	24.46	18.85	24.4	24.85	25.21	27.91	24.62	24.15	24.15	12.53	Si	27.45	26.33
K		0.51	0.34	0.27	0.35	1.62	0.28	0.27	0.27	22.6	K	0.6	0.54
Ca	8.03	13.14	8	8	8.24	2.64	7.88	4.92	4.92	1.83	Ca	6.89	6.72
Fe	0.39	0.26	0.24	0.34	0.42	0.29	0.34	0.35	0.35	4.55	O	48.66	47.09
O	46.21	44.49	45.94	46.45	47.49	48.28	46.22	43.77	43.77	40.7	Fe		0.31
P		4.78								0.25			
Cl		0.32											
Totals	98.55	97.21	97.76	98.89	101.23	101.74	98.43	92.64	93.66	86.45	Totals	102.67	99.61
An	66.14	77.48	67.11	66.06	66.40	23.93	65.39	46.46	46.46	6.55	An	57.27	57.98
Ab	33.86	19.52	30.03	31.71	30.78	61.38	32.28	50.99	50.99	12.56	Ab	37.74	37.36
Or		3.01	2.85	2.23	2.82	14.69	2.32	2.55	2.55	80.89	Or	4.99	4.66

Sample AGSE07														
Plagioclase	Anorthosite													
Analytical point	7		8		1			3	5	7				
Spectrum	1	2	1	2	2	4	5	1	1	1	2	3	4	5
Na	4.65	4.73	4.77	4.57	4.43	9.38	5.86	4.9	4.73	5.61	4.93	4.49	4.99	3.73
Al	14.18	13.76	14.11	13.86	14.93	10.74	1.02	14.2	14.18	13.61	13.89	14.65	13.74	10.72
Si	27.29	26.84	27.39	26.91	27.55	32.97	12.97	27.59	27.44	27.77	27.38	26.6	27.43	29.29
K	0.67	0.5	0.66	0.56	0.32		27.96	0.58	0.5	0.31	0.27	0.13	0.39	5.88
Ca	6.48	6.26	6.43	6.26	7.39	0.27	0.27	6.32	6.49	5.29	6.33	7.03	6.12	0.99
O	48.05	47.06	48.23	47.2	49.22	50.49	4.47	48.41	48.32	47.87	47.84	47.73	47.74	46.4
Fe			0.37				48.4		0.39					0.92
Mg							1.65							0.51
Totals	101.32	99.15	101.96	99.37	103.83	103.85	102.58	102	102.05	100.46	100.64	100.63	100.41	98.44
An	54.92	54.48	54.22	54.96	60.87	2.80	0.79	53.56	55.38	47.19	54.90	60.34	53.22	9.34
Ab	39.41	41.17	40.22	40.12	36.49	97.20	17.19	41.53	40.36	50.04	42.76	38.54	43.39	35.19
Or	5.68	4.35	5.56	4.92	2.64	0.00	82.02	4.92	4.27	2.77	2.34	1.12	3.39	55.47

Sample AGSE07								AGSKSE08						
Plagioclase	Anorthosite							Plagioclas	Matrix				Grey inc.	Grey inc.
Analytical point		9		11	13	15	19	Analytical	3				4.2	5
Spectrum	6	1	2	4	3	1	4	Spectrum	1	2	3	4		
Na	4.14	4.65	4.68	5.82	4.12	4.68	5.06	Na	3.79	3.62	3.85	3.76	2.19	2.54
Al	13.49	13.84	13.75	13.72	15.32	13.75	14.37	Al	15.26	15.05	15.11	15.4	16.37	15.7
Si	26.13	26.95	27.05	28.76	26.76	27.05	27.11	Si	25.19	25.16	25.39	25.15	21.83	22.15
K	0.57	0.57	0.62	0.29	0.28	0.62	0.24	K	0.34	0.35	0.37	0.29		0.01
Ca	6.41	6.46	6.37	5.42	7.81	6.37	6.77	Ca	8.47	8.13	8.31	8.55	10.03	9.58
O	45.89	47.33	47.34	49.22	48.73	47.34	48.17	O	47.04	46.62	47.1	47.13	44.2	44.04
Totals	96.63	99.80	99.81	103.23	103.02	99.81	101.71	Fe						0.47
								Totals	100.09	98.94	100.14	100.29	94.62	94.49
An	57.64	55.31	54.58	47.01	63.96	54.58	56.09	An	67.22	67.19	66.32	67.86	82.08	78.98
Ab	37.23	39.81	40.10	50.48	33.74	40.10	41.92	Ab	30.08	29.92	30.73	29.84	17.92	20.94
Or	5.13	4.88	5.31	2.52	2.29	5.31	1.99	Or	2.70	2.89	2.95	2.30	0.00	0.08

AGSKSE08											
Plagioclase	Matrix										
Analytical point	8						10				
Spectrum	1	2	3	4	5	7	1	2	3	4	5
Na	4.03	4.01	3.81	4.06	3.66	4.06	3.86	4.03	3.94	3.58	3.55
Al	15.02	15.33	15.3	15.1	15.57	15.54	15.07	14.64	14.65	15.07	14.84
Si	26.49	26.46	26	26.23	25.63	26.31	26.07	25.86	25.76	25.2	27.9
K	0.55	0.42	0.35	0.25	0.18	0.15	0.51	0.49	0.53	0.46	0.43
Ca	7.71	7.96	8.61	8.16	8.86	8.27	7.9	7.38	7.9	8.47	8
O	48.13	48.43	48.07	48.04	47.9	48.55	47.7	46.94	47.02	46.83	49.5
Totals	101.93	102.61	102.15	101.83	101.8	102.89	101.11	99.34	99.81	99.61	104.22
An	62.73	64.25	67.42	65.44	69.76	66.27	64.38	62.02	63.86	67.71	66.78
Ab	32.79	32.36	29.84	32.56	28.82	32.53	31.46	33.87	31.85	28.62	29.63
Or	4.48	3.39	2.74	2.00	1.42	1.20	4.16	4.12	4.28	3.68	3.59

SampleAGSKSE09-1														
Plagioclase	Matrix				Matrix					Matrix				
Analytical point	1				2					3				
Spectrum	1.2	1	2	3	4	1 Core	2	3	4 5 Rim		1 Core	2	3	4 Rim
Na	5.51	4.34	4.37	4.16	4.2	4.29	4.18	5.3	4.78	4.15	4.58	4.06	0.57	6.05
Al	15.08	15.36	14.94	14.77	14.3	14.67	15.13	14.35	15.69	15.86	14.5	14.78	18	14.46
Si	28.05	26.71	26.07	25.17	24.91	25.69	25.65	27.52	27.05	26.16	25.38	25.46	20.35	28.02
K	0.72	0.61	0.6	0.62	0.22	0.66	0.45	0.55	0.67	0.5	0.3	0.58	6.46	0.27
Ca	7.38	7.31	7.34	7.34	7.03	6.74	7.86	5.97	7.37	9.33	6.65	7.29	4.21	5.64
O	50.42	48.73	47.67	46.42	45.55	46.79	47.49	48.61	49.67	49.37	46.24	46.73	42.57	49.31
Fe	0.13	0.3	0.35	0.38	0.48	0.53	0.44	0.52	0.55	0.66	0.41	0.48	0.64	0.42
Totals	107.29	103.35	101.35	98.85	96.69	99.37	101.2	102.82	105.77	106.02	98.06	99.38	92.79	104.16
An	54.22	59.62	59.63	60.56	61.40	57.66	62.93	50.51	57.49	66.74	57.68	61.11	37.46	47.16
Ab	40.48	35.40	35.50	34.32	36.68	36.70	33.47	44.84	37.29	29.69	39.72	34.03	5.07	50.59
Or	5.29	4.98	4.87	5.12	1.92	5.65	3.60	4.65	5.23	3.58	2.60	4.86	57.47	2.26

Sample A11 Plagioclase	Matrix			Matrix			Matrix		Matrix	
Analytical point	1			2			4		6	
Spectrum	1	2	3	1	2	3	1	2	1	2
Na	4.53	4.19	4.48	4.38	4.4	4.25	4.41	4.24	4.32	4.48
Al	14.54	14.92	14.82	15.23	14.96	15.4	15.07	15.25	15.37	15.56
Si	26.56	26.27	26.61	26.78	26.92	26.86	26.89	26.57	27.01	26.82
K	0.4	0.47	0.56	0.34	0.45	0.51	0.57	0.45	0.39	0.41
Ca	7.08	7.66	7.35	7.52	7.4	7.84	7.33	7.68	7.65	7.73
Fe	0.61	0.57	0.62	0.55	0.77	0.46	0.58	0.47	0.58	0.58
O	47.85	47.98	48.28	48.81	48.77	49.14	48.78	48.6	49.24	49.29
Totals	101.57	102.06	102.72	103.61	103.67	104.46	103.62	103.26	104.56	104.88
An	58.95	62.18	59.32	61.44	60.41	62.22	59.55	62.09	61.89	61.25
Ab	37.72	34.01	36.16	35.78	35.92	33.73	35.82	34.28	34.95	35.50
Or	3.33	3.81	4.52	2.78	3.67	4.05	4.63	3.64	3.16	3.25

Sample AGSKSE11 Plagioclase	Matrix				
Analytical point	7	8			
Spectrum	1	2	3	4	5
Na	4.05	3.96	4.03	3.99	4.13
Al	15.54	15.42	15.14	15.23	15.06
Si	26.11	26.33	26.2	26.15	26.04
K	0.33	0.31	0.36	0.5	0.47
Ca	8.08	7.93	7.93	7.93	7.89
O	48.59	48.49	48.09	48.14	47.94
Fe	0.64	0.59	0.44	0.53	0.65
Ti	0.20				
Totals	103.54	103.03	102.19	102.47	102.18
An	64.85	65.00	64.37	63.85	63.17
Ab	32.50	32.46	32.71	32.13	33.07
Or	2.65	2.54	2.92	4.03	3.76

Sample AGSKSE11 Plagioclase	Matrix					
Analytical point	6	10				
Spectrum	6	1	2	3	4	5
Na	3.7	4.25	3.99	3.94	3.98	3.78
Al	15.35	14.87	15.17	14.93	14.91	14.99
Si	25.66	25.87	25.85	26.2	26	25.36
K	0.38	0.13	0.42	0.54	0.65	0.48
Ca	8.35	7.58	7.84	7.62	7.55	8.07
O	47.77	47.39	47.77	47.77	47.61	47
Fe	0.67	0.52	0.75	0.44	0.69	0.49
Ti						
Totals	101.88	100.61	101.79	101.44	101.39	100.17
An	67.18	63.38	64.00	62.98	61.99	65.45
Ab	29.77	35.54	32.57	32.56	32.68	30.66
Or	3.06	1.09	3.43	4.46	5.34	3.89

AGSKSE17 Plagioclas	Anorthosite			Matrix				
Analytical	9			11	13	13_2	4	5
Spectrum	1	2	3	4	3	4	1	1
Na	4.71	4.71	4.68	4.01	4.07	4.33	3.88	4.06
Al	15	15.1	15.07	15.83	15.66	16.12	15.4	15.51
Si	28	28.14	27.97	26.94	27.1	27.77	26.24	26.39
K	0.74	0.65	0.76		0.69		0.61	0.38
Ca	7.19	7.14	7.36	8.37	8.42	8.4	8.01	8.12
O	49.91	50.11	49.99	49.51	49.72	50.84	48.43	48.9
Fe							0.59	0.58
P								
Ti								0.2
Total	105.55	105.85	105.83	104.66	105.66	107.46	103.16	103.94
An	56.88	57.12	57.50	67.61	63.88	65.99	64.08	64.65
Ab	37.26	37.68	36.56	32.39	30.88	34.01	31.04	32.32
Or	5.85	5.20	5.94		5.24		4.88	3.03

AGSKSE17						Sample AGSKSE18											
Plagioclase	Anorthosite					Plagioclas	Matrix					Matrix			Anorthosit		
Analytical point	8					Analytical	1					2				3	
Spectrum	1 Core	2	4	5	7 Rim	Spectrum	1	2	3	4	5	1	2	3	1 Rim	2	3
Na	4.33	5.84	4.36	4.47	3.38	Na	4.46	1.79	3.72	4.58	4.13	4.2	4.19	4.08	4.43	4.4	4.59
Al	14.28	26.91	14.24	14.24	13.2	Al	15.67	16.82	15.24	14.57	15.23	14.27	14.7	15.34	14.38	13.96	14.1
Si	27.01	57.18	26.71	27.07	26.72	Si	27.23	23.29	25.23	27.06	25.99	26.44	26.23	25.84	26.71	26.54	26.47
K	0.94	0.96	0.71	0.88	2.95	K	0.41	3.55	0.24	0.64		0.61	0.56	0.36	0.53	0.51	0.52
Ca	6.8	9.98	7.03	6.91	6.36	Ca	7.57	5.63	9.24	6.84	7.68	6.99	7.41	8.15	6.94	6.77	6.62
O	48.05		47.73	48.15	47.06	O	49.71	45.58	47.33	48.25	47.66	47.4	47.62	47.98	47.77	47.04	47.1
Fe	0.5	0.64	0.46	0.54	0.7	Fe	0.32	0.56				0.76	0.46	0.53	0.47	0.18	0.21
P					0.21	Ti		0.5									
Ti						Totals	105.37	97.73	101	101.95	100.7	100.66	101.17	102.28	101.22	99.41	99.61
Total	101.91	101.51	101.24	102.26	100.58	An	60.85	51.32	70.00	56.72	65.03	59.24	60.94	64.73	58.32	57.96	56.44
An	56.34	59.48	58.10	56.36	50.12	Ab	35.85	16.32	28.18	37.98	34.97	35.59	34.46	32.41	37.23	37.67	39.13
Ab	35.87	34.80	36.03	36.46	26.64	Or	3.30	32.36	1.82	5.31	0.00	5.17	4.61	2.86	4.45	4.37	4.43
Or	7.79	5.72	5.87	7.18	23.25												

Sample AGSKSE18						Sample AGSKSE21.1											
Plagioclase						Plagioclas	Megacryst					Megacryst				Megacryst	
Analytical point						Analytical	1					2				3	
Spectrum	4	5	6	7	8 Core	Spectrum	1	2	3	4	5	1	2	3	4	1	2
Na	4.61	4.71	4.94	5.07	5.18	Na	4.47	5.33	5.62	5.75	5.77	4.62	5.38	6.37	5.27	4.11	5.03
Al	14.51	14.59	14.67	15.07	15.66	Al	12.42	13.26	14.52	14.76	14.81	14.5	14.29	13.28	14.99	14.59	14.31
Si	26.98	27.53	27.88	28.19	29.27	Si	23.72	26.81	27.91	28.68	28.89	25.61	26.98	29.22	27.47	24.66	26.43
K	0.43	0.43	0.24	0.37	0.42	K	0.49	0.66	0.52	0.69	0.58	1.21	0.44	0.82	0.26	2.48	0.45
Ca	6.9	6.82	6.95	7.12	7.44	Ca	5.31	5.39	5.99	5.93	5.84	5.41	6.18	4.24	6.55	3.63	6.2
O	48.14	48.89	49.4	50.28	52.27	Fe	1.02	0.36	0.3	0.31	0.44	0.3	0.29	0.23	0.23	0.36	0.22
Fe	0.17	0.35	0.15	0.24	0.48	O	42.14	46.59	49.25	50.4	50.67	46.17	47.96	49.24	49.19	44.57	47.23
Totals	101.74	103.31	104.24	106.34	110.71	Totals	89.56	98.4	104.1	106.52	107	97.82	101.52	103.4	103.96	94.42	99.88
An	57.79	57.02	57.30	56.69	57.06	An	51.70	47.36	49.38	47.94	47.91	48.13	51.50	37.10	54.22	35.52	53.08
Ab	38.61	39.38	40.73	40.37	39.72	Ab	43.52	46.84	46.33	46.48	47.33	41.10	44.83	55.73	43.63	40.22	43.07
Or	3.60	3.60	1.98	2.95	3.22	Or	4.77	5.80	4.29	5.58	4.76	10.77	3.67	7.17	2.15	24.27	3.85

Sample AGSKSE21.1																		
Plagioclase	Megacryst							Megacryst						Matrix		Enclave plagioclase		
Analytical point		4						5						6		6	7	
Spectrum	3	1 Rim	3	4	5	6	8 Core	1	2	3	4	5	1	2	1.2	1	2
Na	5.55	5.98	5.11	5.01	5.22	5.14	5.02	3.89	5.81	4.4	4.33	5.43	5.62	5.95	5.89	4.46	4.09
Al	14.53	15.08	14.73	15.21	14.78	14.63	14.25	16.6	14.2	15.97	15.81	14.56	13.92	14.2	13.93	15.2	15.49
Si	27.64	28.53	27.92	27.66	27.41	27.27	27.24	25.68	28.35	26.36	26.15	27.6	27.88	28.3	28.29	26.28	25.61
K	0.61	0.32	1.12	0.53	0.7	0.7	0.74	0.26	0.75	0.24	0.2	0.51	1.28	0.27	0.14	0.25	0.27
Ca	5.82	6.85	6.19	6.77	6.38	6.23	6.21	8.93	5.33	8.1	7.97	6.04	4.89	5.4	5.6	7.6	8.16
O	48.89	50.9	49.61	49.69	48.98	0.24	48.17	49.03	49.32	49.17	48.66	48.91	48.38	49.23	48.93	48.1	47.69
Fe	0.32	0.33	0.78	0.34	0.38	48.57	0.3	0.15	0.29	0.45	0.26	0.37	0.21	0.26			
Totals	103.37	107.99	105.46	105.22	103.85	102.77	101.93	104.54	104.05	104.67	103.38	103.43	102.18	103.61	102.78	101.89	101.31
An	48.58	52.09	49.84	55.00	51.87	51.62	51.88	68.27	44.83	63.58	63.76	50.42	41.48	46.47	48.15	61.74	65.18
Ab	46.33	45.48	41.14	40.70	42.44	42.58	41.94	29.74	48.86	34.54	34.64	45.33	47.67	51.20	50.64	36.23	32.67
Or	5.09	2.43	9.02	4.31	5.69	5.80	6.18	1.99	6.31	1.88	1.60	4.26	10.86	2.32	1.20	2.03	2.16

Sample AGSKSE21.1																	
Plagioclase	Hybrid matrix			Megacryst				Enclave pl Megacryst									
Analytical point				8	11			12	16								
Spectrum	3	4	5	1	1	1	3	1.2	1	2	3	4	5	6	7	8	9
Na	3.93	4.02	5.03	6.32	6.26	5.69	5.65	4.51	5.62	5.6	5.69	5.45	5.49	6.07	6.15	6.67	6.81
Al	15.7	15.52	14.59	12.94	13.48	13.6	13.77	15.84	14.88	14.96	14.6	15.13	14.91	14.57	14.36	14.25	13.85
Si	25.61	25.73	27.33	29.01	29.26	28.82	28.57	26.86	29.82	30.02	30.2	29.89	30.07	30.47	30.17	30.75	30.9
K	0.19	0.15	0.22	0.47	0.49	0.87	0.63	0.65	0.93	0.95	1	0.82	0.86	0.7	0.49	0.16	0.21
Ca	8.63	8.38	6.35	4.32	4.84	5.24	5.52	7.99	6.44	6.12	5.86	6.46	6.28	5.81	5.78	5.04	4.7
O	47.99	47.89	48.45	48.57	49.54	49.25	49.19	49.71	51.92	52.09	51.92	52.15	52.11	52.24	51.68	52.08	51.81
Fe						0.26	0.33	0.48									
Totals	102.05	101.69	101.97	101.63	103.87	103.73	103.66	106.03	109.61	109.74	109.27	109.9	109.72	109.86	108.63	108.95	108.28
An	67.69	66.77	54.74	38.88	41.76	44.41	46.78	60.76	49.58	48.30	46.69	50.75	49.72	46.18	46.54	42.46	40.10
Ab	30.82	32.03	43.36	56.89	54.01	48.22	47.88	34.30	43.26	44.20	45.34	42.81	43.47	48.25	49.52	56.19	58.11
Or	1.49	1.20	1.90	4.23	4.23	7.37	5.34	4.94	7.16	7.50	7.97	6.44	6.81	5.56	3.95	1.35	1.79

Sample AGSKSE21.1						
Plagioclase						
Analytical point						
Spectrum	10	11	12	13	14	15
Na	5.95	5.77	6.02	0.99	5.52	5.5
Al	14.52	14.72	14.37	10.51	14.28	14.1
Si	29.3	29.01	28.83	31.08	28.08	28.04
K	0.2	0.05	0.06	12.43	0.16	0.2
Ca	6.14	6.3	6	0.4	6.25	6.04
O	50.86	50.67	50.13	47.81	49.14	48.85
Fe						
Totals	106.97	106.52	105.41	103.22	103.43	102.73
An	49.96	51.98	49.67	2.89	52.39	51.45
Ab	48.41	47.61	49.83	7.16	46.27	46.85
Or	1.63	0.41	0.50	89.94	1.34	1.70

Sample: AGSKSE23							
Plagioclas	Megacryst						
Analytical	7.1						
Spectrum	1 Core	2	3	4	5	6	7
Na	2.45	4.18	4.27	4.51	4.31	4.37	4.62
Al	7.49	12.73	13.35	13.73	11.01	11	13.84
Si	14.01	23.11	24.35	25.23	19.53	19.53	25.11
K	0.34	0.43	0.41	0.53	0.29	0.28	0.56
Ca	3.75	5.84	6.11	6.62	3.5	3.47	6.43
O	25.16	41.53	43.63	45.28	61.36	61.35	45.2
Fe	0.41						
Totals	53.61	87.83	92.12	95.9	97.21	97.7	95.74
An	57.34	55.89	56.63	56.78	43.21	42.73	55.38
Ab	37.46	40.00	39.57	38.68	53.21	53.82	39.79
Or	5.20	4.11	3.80	4.55	3.58	3.45	4.82

Sample: AGSKSE23							
Plagioclase				Matrix			Matrix
Analytical point				4.1			5
Spectrum	8	9	10 Rim	1	2	3	2
Na	4.62	3.95	2.41	4.53	4.27	3.95	5.38
Al	13.84	11.55	10.33	13.85	14.08	11.42	13.46
Si	25.11	21.49	16.6	25	24.7	19.23	26.26
K	0.56	0.4	0.24	1.59	0.5	0.33	0.62
Ca	6.43	5.39	5.72	3.88	6.69	3.67	5.21
O	45.2	38.36	31.27	44.26	44.92	61.4	46.04
Fe							0.28
Totals	95.74	81.14	66.58	93.13	95.16	98.8	97.25
An	55.38	55.34	68.34	38.80	58.38	46.16	46.48
Ab	39.79	40.55	28.79	45.30	37.26	49.69	47.99
Or	4.82	4.11	2.87	15.90	4.36	4.15	5.53

Sample AGSKSE23

Plagioclas	Megacryst													
Analytical	3													
Spectrum	1	2	3	4	5	6	7	8	9	10	11	12	13	14
Na	4.95	4.9	4.02	4.9	4.92	4.85	4.94	2.39	7.76	4.39	5.36	7.67	4.42	4.56
Al	14.15	14.38	14.6	14.8	14.93	14.66	15.04	12.09	12.47	13.99	13.77	11.71	13.23	13.46
Si	27.39	27.28	25.66	28.3	28.62	28.26	27.71	22.4	31.11	24.68	27.85	29.91	24.8	25.49
K	0.41	0.58	0.31	0.53	0.61	0.62	0.2	0.78	0.12	0	3.5	0.53	1.72	2.45
Ca	6.57	6.57	9.11	7.08	7.06	6.82	7.17	15.14	2.62	10.2	1	1.88	5.3	3.05
O	48.22	48.32	47.56	50.05	50.54	49.77	49.57	43.61	50.3	46.15	46.95	48.02	44.02	44.32
Mg			0.37					0.45						
Totals	101.69	102.03	101.63	105.66	106.68	104.98	104.63	96.86	104.38	99.41	98.43	99.72	93.49	93.33
An	55.07	54.52	67.78	56.59	56.08	55.49	58.25	82.69	24.95	69.91	10.14	18.65	46.33	30.32
Ab	41.49	40.66	29.91	39.17	39.08	39.46	40.13	13.05	73.90	30.09	54.36	76.09	38.64	45.33
Or	3.44	4.81	2.31	4.24	4.85	5.04	1.62	4.26	1.14	0.00	35.50	5.26	15.03	24.35

Sample AGSKSE23

Plagioclas	Matrix		Megacryst									
Analytical	8.3		13									
Spectrum	1	2	1	2	3	4	5	6	7	8	9	10
Na	5.04	6	4.95	4.99	5.04	4.88	5	4.72	4.45	4.65	3.55	3.91
Al	14.55	13.42	14.4	14.37	14.51	14.54	14.38	14.59	14.88	14.48	14.77	15.12
Si	27.78	28.59	27.65	27.4	27.72	27.38	27.7	26.88	27.34	26.7	25.97	25.73
K	0.46	1.53	0.58	0.47	0.41	0.53	0.47	0.53	0.88	1.48	3.92	1.16
Ca	6.51	4.2	6.56	6.41	6.52	6.88	6.56	7.31	7.07	5.83	3.59	7.59
O	49.04	48.59	48.77	48.55	49.07	48.84	48.94	48.5	49.03	47.88	46.93	47.74
Fe				0.51	0.51	0.53	0.46	0.78	0.36	0.44	1.18	0.7
Ti										0.24	0.21	0.18
Totals	103.38	102.33	102.91	102.7	103.78	103.58	103.51	103.31	104.01	101.7	100.12	102.13
An	54.20	35.81	54.26	54.00	54.47	55.98	54.53	58.20	57.02	48.75	32.46	59.95
Ab	41.97	51.15	40.94	42.04	42.11	39.71	41.56	37.58	35.89	38.88	32.10	30.88
Or	3.83	13.04	4.80	3.96	3.43	4.31	3.91	4.22	7.10	12.37	35.44	9.16

	Mafic enclave	Altered norite	Altered norite	SLM	Monzo norit	IRL-matrix	Altered norite	Norite	Magnetic vein	IRL-matrix	IRL-matrix	Altered norite	Anorthosite
SiO_2	50.16	52.11	50.83	76.63	62.63	18.10	51.24	50.53	10.38	25.46	11.19	47.71	55.91
TiO_2	4.00	1.83	2.62	0.52	1.41	28.21	2.79	2.37	34.42	22.16	33.85	1.31	0.24
$Al2O_3$	14.15	19.54	16.72	11.01	14.25	8.49	19.70	16.83	4.91	11.45	5.08	22.13	25.92
Fe_2O_3	13.81	7.96	10.35	2.77	7.26	36.75	7.41	10.22	44.04	30.20	43.22	6.52	1.09
MnO	0.17	0.09	0.12	0.04	0.11	0.18	0.06	0.12	0.21	0.16	0.21	0.06	0.01
MgO	3.63	4.22	5.58	0.66	1.33	3.87	2.20	5.93	3.72	3.30	4.13	2.88	0.27
CaO	6.83	8.18	7.03	0.49	3.21	3.16	7.57	7.05	1.61	4.39	1.83	11.08	8.52
Na2O	3.53	3.62	2.97	1.66	3.53	1.32	4.13	2.99	0.57	1.90	0.78	3.48	5.83
K2O	1.95	1.27	1.51	4.46	4.29	0.29	1.62	1.09	0.17	0.55	0.24	1.25	0.83
P_2O_5	1.21	0.43	0.62	0.10	0.39	0.10	0.61	0.54	0.07	0.23	0.12	0.14	0.04
Cr_2O_3	0.007	0.028	0.024	0.003	<0.002	0.361	0.015	0.039	0.491	0.316	0.518	0.015	<0.002
Sum	99.55	99.69	99.59	99.69	99.51	99.59	99.69	99.69	99.57	99.61	99.55	99.77	99.82
An	55.483	62.586	61.077	7.413	29.102	66.247	56.832	63.342	68.511	64.181	64.211	70.082	56.126
Ab	28.676	27.697	25.804	25.113	32.004	27.673	31.006	26.864	24.255	27.778	27.368	22.011	38.406
Or	15.841	9.717	13.119	67.474	38.894	6.080	12.162	9.793	7.234	8.041	8.421	7.906	5.468
Sc	20	12	16	7	14	41	11	16	47	34	47	17	<1
Ti	21762	25299	33453	3957	7973	23201	13189	35551	22302	19784	24760	17266	1619
V	213	111	148	41	51	1178	144	150	1417	989	1404	205	14
Cr	47.894	191.576	164.208	20.526		2469.962	102.63	266.838	3359.422	2162.072	3544.156	102.63	
Co	67.4	50.3	54.4	88.6	57.1	55.5	41.5	65.8	86.8	60.4	88.2	41.9	35.2
Ni	26.7	23.3	71.3	5.6	1.9	47.9	39.0	66.8	174.6	42.6	33.3	35.4	3.3
Cu	23.2	18.7	51.4	6.9	8.5	25.6	61.5	40.6	40.1	22.0	20.1	12.9	4.4
Zn	79	30	41	41	77	8	50	73	11	9	10	24	5
Ga	26.3	24.4	22.2	11.1	25.3	16.8	23.4	19.0	14.2	19.4	15.8	19.7	15.7
Rb	49.0	28.5	41.7	134.7	85.0	4.1	37.1	31.0	2.8	10.2	5.3	36.9	6.6
Sr	547.0	672.4	602.5	132.8	315.8	307.8	727.9	561.5	157.1	424.6	172.7	736.2	997.9

Y	61.2	24.5	34.1	28.2	80.9	6.3	32.4	28.9	5.2	10.3	6.5	9.3	1.8
Zr	545.9	203.7	278.0	325.6	955.9	306.4	219.1	251.2	360.6	289.0	365.9	61.0	9.8
Nb	27.7	10.2	13.5	13.0	30.8	32.9	9.5	11.9	36.7	28.4	38.2	2.6	0.4
Cs	0.4	0.7	4.1	8.1	2.7	0.1	1.8	2.4	0.3	<0.1	<0.1	4.7	<0.1
Ba	952	479	576	893	1387	175	668	346	79	272	128	264	210
La	72.6	26.1	39.0	39.3	78.0	7.7	41.1	34.5	4.7	14.0	8.0	9.2	2.7
Ce	161.6	56.2	85.3	81.9	183.7	15.9	92.0	74.9	9.8	29.5	16.8	18.9	4.7
Pr	20.66	7.21	11.27	9.70	23.95	1.91	11.63	9.91	1.28	3.89	2.15	2.54	0.58
Nd	85.9	30.7	47.6	36.0	101.3	8.4	47.8	42.2	5.3	15.1	9.2	12.0	2.5
Sm	17.19	6.44	9.42	6.33	20.03	1.60	9.40	8.14	1.05	2.97	1.68	2.50	0.45
Eu	4.47	2.04	2.50	1.07	4.51	0.70	2.48	2.37	0.41	1.13	0.57	1.00	0.69
Gd	16.23	6.15	8.43	5.39	18.56	1.37	8.55	7.32	1.02	2.90	1.68	2.51	0.45
Tb	2.34	0.93	1.24	0.90	2.98	0.21	1.26	1.08	0.16	0.40	0.24	0.39	0.06
Dy	12.41	5.18	6.98	5.41	16.61	1.16	6.64	5.99	0.99	2.33	1.41	1.99	0.31
Ho	2.19	0.87	1.19	1.04	3.06	0.21	1.12	1.04	0.20	0.43	0.25	0.40	0.05
Er	5.90	2.30	3.37	3.13	8.45	0.69	3.07	2.83	0.63	1.12	0.79	1.09	0.14
Tm	0.82	0.34	0.47	0.50	1.27	0.10	0.44	0.42	0.09	0.16	0.11	0.14	0.02
Yb	5.15	2.08	2.88	3.25	7.73	0.77	2.50	2.48	0.76	1.08	0.88	0.85	0.10
Lu	0.74	0.31	0.43	0.55	1.19	0.14	0.37	0.40	0.13	0.18	0.14	0.12	0.02
Hf	4.7	6.7	9.1	22.8	8.5	5.7	6.3	9.9	7.7	9.5	1.6	0.3	9.4
Ta	0.8	1.0	1.7	2.1	0.7	0.7	2.6	2.0	2.9	0.2	<0.1	2	
Pb	1.4	1.5	2.3	8.6	13.8	1.4	3.9	1.9	2.0	1.3	1.4	1.3	0.4
Th	4.9	2.0	3.6	14.5	5.8	0.5	3.9	3.2	0.3	1.1	0.6	0.6	<0.2
U	1.2	0.6	0.8	3.9	3.0	0.2	0.9	0.8	<0.1	0.3	0.2	0.2	<0.1
Au (ppb)	0.9	1.9	1.3	1.9	<0.5	5.8	1.3	1.2	5.7	1.9	4.4	1.2	0.7

Tidigare skrifter i serien ”Examensarbeten i Geologi vid Lunds universitet”:

403. Kall, Christoffer, 2014: Microscopic echinoderm remains from the Darriwilian (Middle Ordovician) of Västergötland, Sweden – faunal composition and applicability as environmental proxies. (15 hp)
404. Preis Bergdahl, Daniel, 2014: Geoenergi för växthusjordbruk – Möjlig anläggning av värme och kyla i Västskåne. (15 hp)
405. Jakobsson, Mikael, 2014: Geophysical characterization and petrographic analysis of cap and reservoir rocks within the Lund Sandstone in Kyrkheddinge. (15 hp)
406. Björnfors, Oliver, 2014: A comparison of size fractions in faunal assemblages of deep-water benthic foraminifera—A case study from the coast of SW-Africa.. (15 hp)
407. Rådman, Johan, 2014: U-Pb baddeleyite geochronology and geochemistry of the White Mfolozi Dyke Swarm: unravelling the complexities of 2.70-2.66 Ga dyke swarms on the eastern Kaapvaal Craton, South Africa. (45 hp)
408. Andersson, Monica, 2014: Drumliner vid moderna glaciärer — hur vanliga är de? (15 hp)
409. Olsenius, Björn, 2014: Vinderosion, sanddrift och markanvändning på Kristianstadsslätten. (15 hp)
410. Bokhari Friberg, Yasmin, 2014: Oxygen isotopes in corals and their use as proxies for El Niño. (15 hp)
411. Fullerton, Wayne, 2014: REE mineralisation and metasomatic alteration in the Olserum metasediments. (45 hp)
412. Mekhaldi, Florian, 2014: The cosmic-ray events around AD 775 and AD 993 - Assessing their causes and possible effects on climate. (45 hp)
413. Timms Eliasson, Isabelle, 2014: Is it possible to reconstruct local presence of pine on bogs during the Holocene based on pollen data? A study based on surface and stratigraphical samples from three bogs in southern Sweden. (45 hp)
414. Hjulström, Joakim, 2014: Bortforsling av kaxblandat vatten från borrningar via dagvattenledningar: Riskanalys, karaktärisering av kaxvatten och reningsmetoder. (45 hp)
415. Fredrich, Birgit, 2014: Metadolerites as quantitative P-T markers for Sveconorwegian metamorphism, SW Sweden. (45 hp)
416. Alebouyeh Semami, Farnaz, 2014: U-Pb geochronology of the Tsineng dyke swarm and paleomagnetism of the Hartley Basalt, South Africa – evidence for two separate magmatic events at 1.93-1.92 and 1.88-1.84 Ga in the Kalahari craton. (45 hp)
417. Reiche, Sophie, 2014: Ascertaining the lithological boundaries of the Yoldia Sea of the Baltic Sea – a geochemical approach. (45 hp)
418. Mroczek, Robert, 2014: Microscopic shock-metamorphic features in crystalline bedrock: A comparison between shocked and unshocked granite from the Siljan impact structure. (15 hp)
419. Balija, Fisnik, 2014: Radon ett samhällsproblem - En litteraturstudie om geologiskt sammanhang, hälsoeffekter och möjliga lösningar. (15 hp)
420. Andersson, Sandra, 2014: Undersökning av kalciumkarbonatförekomsten i infiltrationsområdet i Sydvattens vattenverk, Vombverket. (15 hp)
421. Martin, Ellinor, 2014: Chrome spinel grains from the Komstad Limestone Formation, Killeröd, southern Sweden: A high-resolution study of an increased meteorite flux in the Middle Ordovician. (45 hp)
422. Gabrielsson, Johan, 2014: A study over Mg/Ca in benthic foraminifera sampled across a large salinity gradient. (45 hp)
423. Ingvaldson, Ola, 2015: Ansvarsutredningar av tre potentiellt förorenade fastigheter i Helsingborgs stad. (15 hp)
424. Robygd, Joakim, 2015: Geochemical and palaeomagnetic characteristics of a Swedish Holocene sediment sequence from Lake Storsjön, Jämtland. (45 hp)
425. Larsson, Måns, 2015: Geofysiska undersökningsmetoder för geoenergisystem. (15 hp)
426. Hertzman, Hanna, 2015: Pharmaceuticals in groundwater - a literature review. (15 hp)
427. Thulin Olander, Henric, 2015: A contribution to the knowledge of Fårö's hydrogeology. (45 hp)
428. Peterffy, Olof, 2015: Sedimentology and carbon isotope stratigraphy of Lower–Middle Ordovician successions of Slemmestad (Oslo-Asker, Norway) and Brunflo (Jämtland, Sweden). (45 hp)

429. Sjunnesson, Alexandra, 2015: Spårämnesförsök med nitrat för bedömning av spridning och uppehållstid vid återinfiltrationav grundvatten. (15 hp)
430. Henao, Victor, 2015: A palaeoenvironmental study of a peat sequence from Iles Kerguelen (49° S, Indian Ocean) for the Last Deglaciation based on pollen analysis. (45 hp)
431. Landgren, Susanne, 2015: Using calcein-filled osmotic pumps to study the calcification response of benthic foraminifera to induced hypoxia under *in situ* conditions: An experimental approach. (45 hp)
432. von Knorring, Robert, 2015: Undersökning av karstvittring inom Kristianstadsslättens NV randområde och bedömning av dess betydelse för grundvattnets sårbarhet. (30 hp)
433. Rezvani, Azadeh, 2015: Spectral Time Domain Induced Polarization - Factors Affecting Spectral Data Information Content and Applicability to Geological Characterization. (45 hp)
434. Vasilica, Alexander, 2015: Geofysisk karaktärisering av de ordoviciska kalkstensenheterna på södra Gotland. (15 hp)
435. Olsson, Sofia, 2015: Naturlig nedbrytning av klorerade lösningsmedel: en modellering i Biochlor baserat på en fallstudie. (15 hp)
436. Huitema, Moa, 2015: Inventering av föroreningar vid en brandövningsplats i Linköpings kommun. (15 hp)
437. Nordlander, Lina, 2015: Borrningsteknikens påverkan vid provtagning inför dimensionering av formationsfilter. (15 hp)
438. Fennvik, Erik, 2015: Resistivitet och IP-mätningar vid Äspö Hard Rock Laboratory. (15 hp)
439. Pettersson, Johan, 2015: Paleoekologisk undersökning av Triberga mosse, sydöstra Öland. (15 hp)
440. Larsson, Alfred, 2015: Mantelplymer - realitet eller *ad hoc*? (15 hp)
441. Holm, Julia, 2015: Markskador inom skogsbruket - jordartens betydelse (15 hp)
442. Åkesson, Sofia, 2015: The application of resistivity and IP-measurements as investigation tools at contaminated sites - A case study from Kv Renen 13, Varberg, SW Sweden. (45 hp)
443. Lönsjö, Emma, 2015: Utbredningen av PFOS i Sverige och världen med fokus på grundvattnet – en litteraturstudie. (15 hp)
444. Asani, Besnik, 2015: A geophysical study of a drumlin in the Åsnen area, Småland, south Sweden. (15 hp)
445. Ohlin, Jeanette, 2015: Riskanalys över pesticidförekomst i enskilda brunnar i Sjöbo kommun. (15 hp)
446. Stevic, Marijana, 2015: Identification and environmental interpretation of microtextures on quartz grains from aeolian sediments - Brattforsheden and Vittskövle, Sweden. (15 hp)
447. Johansson, Ida, 2015: Is there an influence of solar activity on the North Atlantic Oscillation? A literature study of the forcing factors behind the North Atlantic Oscillation. (15 hp)
448. Halling, Jenny, 2015: Inventering av sprickmineraliseringar i en del av Sorgenfrei-Tornquistzonen, Dalby stenbrott, Skåne. (15 hp)
449. Nordas, Johan, 2015: A palynological study across the Ordovician Kinnekulle. (15 hp)
450. Åhlén, Alexandra, 2015: Carbonatites at the Alnö complex, Sweden and along the East African Rift: a literature review. (15 hp)
451. Andersson, Klara, 2015: Undersökning av slugtestsmetodik. (15 hp)
452. Ivarsson, Filip, 2015: Hur bildades Bushveldkomplexet? (15 hp)
453. Glommé, Alexandra, 2015: $^{87}Sr/^{86}Sr$ in plagioclase, evidence for a crustal origin of the Hakefjorden Complex, SW Sweden. (45 hp)

LUNDS UNIVERSITET

Geologiska institutionen
Lunds universitet
Sölvegatan 12, 223 62 Lund